

**DEVELOPMENT AND CHARACTERIZATION OF
ELECTROSPUN CARBON NANOFIBERS
FOR PROTON EXCHANGE MEMBRANE FUEL CELLS**

by
CENK GÜMECİ

**Submitted to the Graduate School of Engineering and Natural Sciences
in partial fulfillment of the requirements for the degree of
Master of Science**

Sabancı University

Fall 2007

DEVELOPMENT AND CHARACTERIZATION OF
ELECTROSPUN CARBON NANOFIBERS
FOR PROTON EXCHANGE MEMBRANE FUEL CELLS

APPROVED BY

Assoc. Prof. Yusuf Menceloğlu
(Thesis Supervisor)

Prof. Atilla Güngör

Prof. Baki Hazer

Asst. Prof. Melih Papila

Asst. Prof. Alpay Taralp

Asst. Prof. Mehmet Yıldız
(Substitute Member)

DATE OF APPROVAL: 12/02/2008

© Cenk Gümece 2008
All Rights Reserved

**To my twin brother
Cem Gümeçi**

ACKNOWLEDGMENTS

First, I would like to thank my advisor Yusuf Z. Mencelođlu for his limitless patience, continuous support and encouragement throughout this research.

My sincere thanks go to my colleague Burak Birkan for his endless help, trust and brotherhood.

I would also like to thank Melih Papila, Mehmet Ali Glgn, Yuda Yrm and Alpay Taralp for their kind comments and suggestions during this research.

My special thanks to my friends, “Murat Giray, Burcu Saner, Emre Fırlar, Fatih Tabak, Vanya Uluç, Didem Çilingir, Seren Yksel, Glay Bozoklu, Funda İnceođlu, Aslı Nalbant, zge Malay, Ayça Erden, and Canan Barıřtıran” for their friendship and support. I would also like to thank my room mate Serhat Tosun at Sabancı University dorm for his kind friendship and sense of humor.

I would like to express my gratitude to my family; Hatice, Fahri, Ececan and Ayçe for their endless love and support.

Finally, I would like to thank my love, zz, with all my heart for her trust, encouragement, patience and endless love.

**DEVELOPMENT AND CHARACTERIZATION OF
ELECTROSPUN CARBON NANOFIBERS
FOR PROTON EXCHANGE MEMBRANE FUEL CELLS**

ABSTRACT

In this work, electrospinning was used to produce acrylonitrile based copolymer carbon nanofibers (CNFs) with Platinum (Pt) and Palladium (Pd) nanoparticles for use in proton exchange membrane fuel cells (PEMFC). Acrylonitrile was copolymerized with n-vinyl pyrrolidinone (VPYR) with different ratios as a template the size and the distribution of nanoparticles. The polymer, metal salt and solvent mixture were electrospun for producing metal salt bearing polymeric nanofibers. Polymeric nanofibers were then dipped in a reducing solvent to produce metal nanoparticle on/in the polymer nanofibers. In order to get carbon fiber, pyrolysis were conducted which was performed by heat treatment process that includes stabilization of electrospun nanofibers in air environment at 200 °C followed by carbonization in nitrogen environment to temperatures between 600 °C and 1200 °C with different heating rates. The diameters of carbon nanofibers were found in the range of 80 to 600 nanometers while the particle sizes were reduced up to 4 nanometers. The electrocatalytic surface area was achieved as 34,5m²/g for Pt and 22,4m²/g for Pd nanoparticles. Synthesized polymers were characterized by Fourier Transform Infrared Spectroscopy (FTIR), Nuclear Magnetic Resonance (NMR), Simultaneous Thermal Analysis (STA) and Differential Scanning Calorimetry (DSC). Fiber morphologies and nanoparticle sizes were examined via Scanning Electron Microscopy (SEM), X-Ray Diffractometer (XRD) and Tunneling Electron Microscopy (TEM). Electrochemical performance of metal nanoparticles was evaluated by means of cyclic voltammetry (CV).

**PROTON DEĞİŞİMLİ MEMBRAN YAKIT PİLLERİ İÇİN
NANOKARBON FİBERLERİN GELİŞTİRMELERİ
VE KARAKTERİZASYONLARI**

ÖZET

Bu çalışmada, proton değişimli membran yakıt hücreleri için elektro dokuma yöntemiyle poliakrilonitril kökenli Platin (Pt) ve Paladyum (Pd) nanoparçacık içeren karbon nanofiberler sentezlenmiştir. Nano metal parçacıkların küçük parçacık boyutu ve düzgün dağılımlarının sağlanması için, fonksiyonel poli akrilonitril, n-vinil payrolidon ile değişik mol oranlarında kopolimerleşmiştir. Sentezlenen polimer, çözücü ve metal tuzundan oluşan viskos çözelti elektro dokuma yöntemiyle, metal tuzu içeren nanofiberlere dönüştürülmüştür.. Metal nanoparçacık eldesi için polimerik nanofiberler, indirgen çözücüde bekletilmişlerdir. Karbon fiber eldesi için karbonizasyon iki etapta gerçekleşmiştir. İlk olarak, fiberler oksijen ortamında 200 °C de stabilize hale getirilmişlerdir. Bunu, azot atmosferinde 600 °C ile 1200 °C sıcaklıklarında ve değişik ısıtma hızlarında uygulanan yakma işlemi takip etmiştir.

Karbon nanofiber çapları 80-600 nanometre arasında ölçülmüşken, metal parçacık boyutu 4 nanometreye kadar düşürülmüştür. Azami elektroaktif yüzey alanı Pt nanoparçacık için 34,5 m²/g Pd nanoparçacık için ise 22,37 olarak bulunmuştur. Sentezlenen polimerler, Fourier Transform Kızılötesi Spektroskopisi (FTIR), Nükleer Manyetik Rezonans Spektroskopisi (NMR), Anlık Termal Analiz (STA) ve Diferansiyel Taramalı Kalorimetri (DSC) teknikleriyle karakterize edilmişlerdir. Fiber morfolojisi ile metal nanoparçacık boyutları Taramalı Electron Mikroskobu (SEM), X-Ray difraktometre (XRD) ve Geçirmeli Elektron Mikroskobu (TEM) ile incelenmiştir. Nanoparçacıkların elektrokimyasal analizleri dönüşümlü voltametre (CV) ile gerçekleştirilmiştir.

TABLE OF CONTENTS

1. INTRODUCTION.....	1
1.1. Fuel Cell Fundamentals.....	1
1.1.1. Why Fuel Cells?	1
1.1.2. Fuel Cell Definition.....	2
1.1.3. Fuel Cell Electrochemistry.....	3
1.1.4. Main Advantages of Fuel Cells.....	3
1.1.5. Disadvantages of Fuel Cells.....	4
1.2. Fuel Cell Types.....	4
1.2.1. Polymer Electrolyte Membrane Fuel Cells (PEMFC).....	5
1.3. PEMFC Working Principles.....	6
1.4. Main PEMFC Components.....	8
1.4.1. Membrane.....	8
1.4.2. Electrode.....	9
1.4.3. Gas Diffusion Layer.....	10
1.4.4. Bipolar Plate.....	11
1.5. Motivation.....	11
1.6. Electrospinning.....	12
2. EXPERIMENTAL.....	15
2.1. Materials.....	15
2.2. The Synthesis of Polyacrylonitrile Copolymers.....	16
2.3. Electrospinning of Metal Containing Polymer Solutions.....	16
2.4. The Reduction of Metals.....	19
2.5. Heat Treatments.....	19
2.6. Characterization of Polyacrylonitrile copolymers.....	20
2.7. Characterization of Fibers	21
2.7.1. Optical Microscopy.....	21
2.7.2. X-Ray Diffraction (XRD).....	21
2.7.3. Scanning Electron Microscopy (SEM).....	22
2.7.4. Tunneling Electron Microscopy (TEM).....	23
2.8. Cyclic Voltammetry (CV).....	23

2.8.1. Electrochemical Testing Setup.....	25
2.8.2. Electrode Preparation.....	26
3. RESULTS AND DISCUSSION.....	27
3.1. The Synthesis of Polyacrylonitrile Copolymers via Solution Polymerization...27	
3.2. Structural Characterization.....	28
3.2.1. NMR Characterizations	28
3.2.2. FT-IR Characterizations of P (AN-co-VPYR).....	31
3.3. Thermal Characterization.....	32
3.4. Electrospinning Characterization.	35
3.4.1. Sample SEM Images (Concentration Effect).....	38
3.5. Reduction Characterization.....	39
3.6. Carbonization Characterization.....	41
3.6.1. Sample SEM Images (Heat Treatment Effect).....	41
3.7. Characterization of Pt Including Fibers.....	42
3.7.1. Sample SEM Images (Carbonization Temperature Effect).....	44
3.8. Characterization of Pd Including fibers.....	45
3.8.1. Sample TEM Images (Heating Rate Effect).....	47
3.9. XRD Analysis.....	48
3.9.1. XRD Analysis of Pt Including Fibers.....	48
3.9.2. XRD Analysis of Pd Including Fibers.....	51
3.10. Electrochemical Results.....	53
3.10.1. Electrochemical Analysis of Pt Including Fibers.....	53
3.10.2. Electrochemical Analysis of Pd Including Fibers.....	57
4. CONCLUSION and FUTURE WORKS.....	61
REFERENCES.....	63
APPENDIX.....	70

LIST OF FIGURES

Figure 1.1. A typical fuel cell.....	2
Figure 1.2. A typical polymer electrolyte fuel cell sheme.....	7
Figure 1.3. A schematic diagram of electrospinning setup.....	13
Figure 1.4. Electrospinning process parameters.....	14
Figure 2.1. Figure of typical home-made electrospinning setup.....	17
Figure 2.2. Figure of 10 X 10 cm ² aluminum mesh metal collector.....	18
Figure 2.3. Heat treatment ramp rate: 40 ⁰ C/min	20
Figure 2.4. Debye Scherer Formul.....	22
Figure 2.5. A typical cyclic voltammogram.....	24
Figure 2.6. Three electrode electrochemical working cell.....	26
Figure 3.1. Chemical srtuctures of copolymers.....	28
Figure 3.2. H-NMR of P (AN co VPYR).....	29
Figure 3.3. H-NMR of P (AN co AA).....	30
Figure 3.4. FT-IR of P (An-co-5% VPYR).....	31
Figure 3.5. P (An-co-AA), DSC analysis.....	32
Figure 3.6. P (AN-co-VPYR), DSC analysis.....	33
Figure 3.7. STA of P (An-co-VPYR).....	34
Figure 3.8. SEM images of P(AN-co- 5% VPYR) - 20, 15, 5 % weight polymer solution concentrations.....	38
Figure 3.9. Reducing reactions: Gas evolution and color change of fiber mat before and after the reaction.....	39
Figure 3.10. Reducing agent comparasion.....	40
Figure 3.11. SEM images of P (AN-co-%5 VPYR) before and after carbonization.....	41
Figure 3.12. SEM images of P(AN-co-5%VPYR)-20%Pt carbonized at 600 ⁰ C and 1000 ⁰ C.....	44
Figure 3.13. . P(AN-co-%5-VPYR), 5%Pd 600C, 5 ⁰ C/min heating rate Figure3d P(AN-co-%5-VPYR), 5%Pd 600C, 1 ⁰ C/min heating rate.....	47
Figure 3.14. XRD spectrum of P (AN-5% VPYR)-20% P+ carbonized at 600 ⁰ C.....	49

Figure 3.15-16. P(AN-5%VPYR)-20%Pt 600C-40C/min with reducing agent and without reducing agent.....	50
Figure 3.17. %20 Pd carbonized at 1000 ⁰ C.....	52
Figure 3.18. %20 Pd carbonized at 600 ⁰ C.....	52
Figure 3.19. Cyclic Voltammogram of 20% Pt including carbon fiber.....	54
Figure 3.20. P(AN-%5VPYR)-20%Pt 600 ⁰ C 40 ⁰ C/min.....	55
Figure 3.21. The behavior of Pt catalyst in oxygen saturated solution.....	57
Figure 3.22. Cyclic voltammogram of slightly defined adsorption and desorption regions for hydrogen of Pd nanoparticles on carbon fibers at 10mV/s scan rate in 0.5M H ₂ SO ₄	58
Figure 3.23. Cyclic voltammograms of P (AN-co-VPYR) carbon nanofibers a) at increasing Pd concentration (%5 Pd, %20 Pd in weight with respect to polymer b) at various heating rates (0.1 ⁰ C/min, 10 ⁰ C/min, 50 ⁰ C/min).....	59
Figure A.1. (a) 0.1 ⁰ C/min heating rate, (b) 1 ⁰ C/min heating rate for P(AN-co-%5-VPYR), 5%Pd 600 ⁰ C.....	70
Figure A.2. P(AN-co-%5-VPYR), 20%Pd 600 ⁰ C- 40 ⁰ C/min, 2 distrubitions.....	71
Figure A.3. P(AN-co-%5-VPYR), 20%Pt 600 ⁰ C- 40 ⁰ C/min, different magnification..	72
Figure A.4. P(AN-co-%5-VPYR), 20%Pt 600 ⁰ C- 40 ⁰ C/min, bead formation, 8% polymer concentration (lower polymer concentration).....	73
Figure A.5. P(AN-co-%5-VPYR), 20%Pt 600 ⁰ C- 40 ⁰ C/min, unreduced, smooth fiber formation , 15% polymer concentration (higher polymer concentration).....	73
Figure A.6. TEM of P(AN-co-%5-VPYR), 20%Pd 1000 ⁰ C- 40 ⁰ C/min, 2 distrubitions 3-5 nm, 20-40 nm.....	74

LIST OF TABLES

Table 2.1. Summary of the electrospinning working condition.....	18
Table 3.1. Thermal and NMR analysis results.....	34
Table 3.2. Fiber diameter of P(AN-co-AA). 1: Functional monomer ration in polymer, 2: Weight percentage of metal in polymer. 2: Weight percentage of polymer in solution.....	36
Table 3.3. Fiber diameter of P(AN-co-VPYR). 1: Functional monomer ration in polymer, 2: Weight percentage of metal in polymer. 3: Weight percentage of polymer in solution.....	37
Table 3.4. P(AN-co-5%VPYR)- 5%-Pd and P(AN-co-5%VPYR)-5%-Pt carbonized at 1000 ⁰ C.....	40
Table 3.5. P(AN-5%VPYR) -%Pt carbonized at 600 ⁰ C.....	43
Table 3.6. P(AN-co-5%VPYR)-5%Pd, Different carbonization temperatures and rates.....	46
Table 3.7. Pt including copolymers with different comonomer and Pt ratios.....	51
Table 3.8. Summary of electrochemical results for Pt including fiber.....	56
Table 3.9. Summary of electrochemical results for Pd including fiber.....	60

LIST OF ABBREVIATIONS

PEMFC	:	Proton Exchange Membrane Fuel Cell
MEA	:	Membrane Electrode Assembly
PFPE	:	Polytetrafluoroethylene
ORR	:	Oxygen Reduction Reaction
FT-IR	:	Fourier Transform Infrared Spectroscopy
NMR	:	Nuclear Magnetic Resonance
DSC	:	Differential Scanning Calorimetry
STA	:	Simultaneous Thermal Analysis
SEM	:	Scanning Electron Microscopy
TEM	:	Tunneling Electron Microscopy
XRD	:	X-Ray Diffractometer
T _g	:	Glass Transition Temperature
T _m	:	First Decomposition Temperature
CV	:	Cyclic Voltammetry

CHAPTER 1

INTRODUCTION

1.1. Fuel Cell Fundamentals

1.1.1. Why Fuel Cells?

The fossil fuels, petroleum, and natural gas meet about 80% of the world energy demand today. However there are two crucial problems related with continued use of fossil fuels. The first one is that they are limited in amount and sooner or later will be depleted. The second one is that fossil fuels cause serious environmental problems, such as global warming, climate changes, ozone layer depletion and so on. Therefore, other energy sources such as hydrogen, sun, wind and so on should be used instead of fossil fuels. At this point, fuel cells, which are cleaner, cheaper and more efficient energy systems may be a solution of the mankind energy demands for very near future [1].

1.1.2. Fuel Cell Definition

The first fuel cell was developed by Welsh scientist Sir William Robert Grove in 1839 [2]. He reversed the electrolysis of the water to generate electricity from combining of hydrogen and oxygen. Since then, the basic principle of a fuel cell remains unchanged today. Specifically, a fuel cell is an electrochemical cell which can directly convert the chemical energy of fuel into electrical energy by a process involving an electrode – electrolyte system. The fuel cell consists of two electrodes: anode and cathode. At the anode the fuel (mostly hydrogen, methanol or hydrazine) is oxidized, at the cathode where the reduction (usually oxygen) takes place. Figure1.1. illustrates a typical fuel cell configuration.

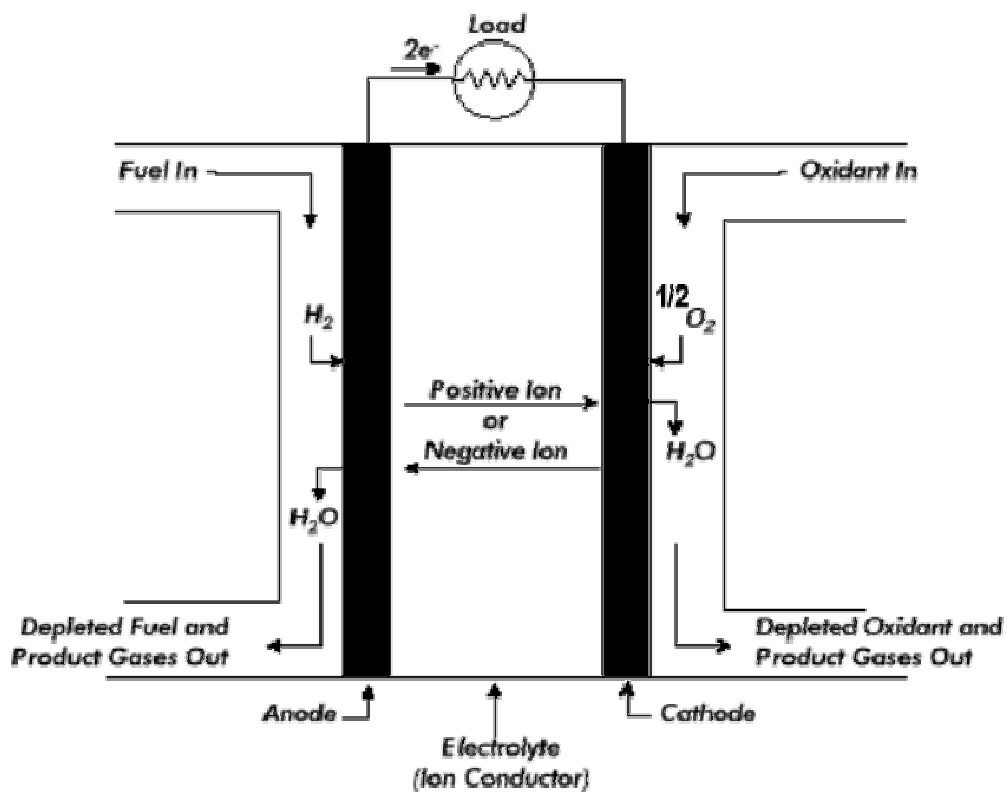


Figure1.1. A typical fuel cell [3]

A fuel cell is in some aspects similar to a battery. It has an electrolyte, positive and negative electrodes and it generates electricity. However, in the case of a battery, the chemical energy is stored in a closed system. The battery must be thrown away when

the chemical energy is converted to electrical energy. In the case of a fuel cell, the chemical energy is provided by a fuel and an oxidant stored outside where the chemical reactions take place. As long as the cell is supplied with fuel and oxidant, electrical energy can be obtained. In addition to these, electrodes within a battery react and change as charged or discharged, while a fuel cell's electrodes are relatively stable.

1.1.3. Fuel Cell Electrochemistry

The basic physical structure of all fuel cells consists of an electrolyte layer in contact with an anode and cathode electrode on either side of the electrolyte. The electrolyte allows the conduction of ionic charge between the electrodes, and transports the dissolved reactants to the electrode. Moreover, the electrolyte provides a physical barrier to prevent the direct mixing of the fuel and the oxidant. The electrode structure is porous, and the electrode is used to maximize the three-phase interface between the electrode, electrolyte and gas/liquid. Furthermore, it separates the bulk gas phase and the electrolyte. The gas/liquid ionization or de-ionization reactions take place on the surface of the electrode, and the reactant ions are conducted away from or into three – phase interface. In theory a fuel cell is capable of producing an electric current so long as it is supplied with fuel. However, fuel cell performance will gradually deteriorate over a period of time when the electrode and electrolyte age are increased [4].

1.1.4. Main Advantages of Fuel Cells

Fuel cells are generally more efficient than combustion engines. Because they are not limited by temperature as is heat engine. In fuel cells, chemical energy is converted directly into electricity without preliminary conversion into heat. In addition, no mechanical conversion is required [5].

Fuel cells have essentially simple few or no moving parts. High reliability may be attained with operational lifetimes exceeding 40,000 hours in which the operational life is formally over when rated power of the fuel cell is no longer satisfied [6].

In most fuel cells end products are water (for hydrogen fuel cells), carbon dioxide or nitrogen and as well as heat. Therefore, fuel cells can be classified as clean energy sources. The operation of fuel cell systems is very quiet because it has no or few moving parts. Modular installations can be used to match the load and increase the reliability of the system [7].

1.1.5. Disadvantages of Fuel Cells

The main disadvantages of fuel cells are their relatively high cost and to have a less extent the source of the fuel comparing fossil fuels. For stationary application (large scale system) systems a cost of 1000 dollars per kW and operation life of 40,000 hours is required. The current cost of a fuel cell for large scale is around 3000 dollars per kW [8,9].

1.2. Fuel Cell Types

Fuel cell types are generally characterized by electrolyte material. An electrolyte is the substance between the positive and negative terminals, serving as the bridge for the ion exchange that generates electrical current [10]. There are five different fuel cell types. These five fuel cell types are significantly different from each other in many respects; however, the key distinguishing feature is the electrolyte material. These are proton exchange membrane fuel cell (also called polymer electrolyte membrane fuel cell), alkaline fuel cell, phosphoric acid fuel cell, molten carbonate fuel cell and solid oxide fuel cell [11]. In this study, only Proton Exchange Membrane Fuel Cells (PEMFCs) will be focused and explained in detail.

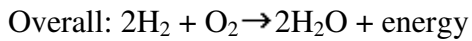
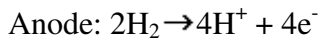
1.2.1. Proton Exchange Membrane Fuel Cells (PEMFC)

This technology was invented by General Electric in the 1950s and was used by NASA to provide power for the Gemini space project [12]. PEM fuel cells are also known as polymer electrolyte membrane fuel cell, solid polymer electrolyte and polymer electrolyte fuel cells. PEM fuel cells have a number of attributes that make them ideal candidates for use in automotive applications and small domestic applications, such as replacements for rechargeable batteries. They operate at relatively low temperatures which allows them to start up rapidly from cold and have a high power density which makes them relatively compact. In addition, PEM cells work at high efficiencies, producing around 40-50 per cent of the maximum theoretical voltage, and can vary their output quickly to meet shifts in power demand [13].

At present, demonstration units capable of producing 50 kW are in operation and units producing up to 250 kW are under development. There are, however, still a number of barriers that need to be resolved before this technology becomes more widespread. The main issue is the cost of the membrane materials and catalysts. The other drawback of PEM cells is that they need pure hydrogen to operate as they are very susceptible to poisoning by carbon monoxide and other impurities. This is largely due to the low operating temperature of the cell which necessitates the use of a highly sensitive catalyst. Again, work is being carried out to produce more tolerant catalyst systems along with membranes capable of operating at higher temperatures [14].

1.3. PEMFC Working Principles

In the PEM fuel cell the electrolyte is a thin polymer membrane (such as poly[perfluorosulphonic] acid, NafionTM which is permeable to protons, but does not conduct electrons, and the electrodes are typically made from carbon. Hydrogen flows into the fuel cell at the anode side and is split into hydrogen ions (protons) and electrons. The hydrogen ions permeate across the electrolyte to the cathode, while the electrons flow through an external circuit and provide power. Oxygen, in the form of air, is supplied to the cathode and combines with the electrons and the hydrogen ions thereby producing water [15]. These reactions at the electrodes are as follows:



Schematic of a single typical proton exchange membrane fuel cell is shown in figure 1.2

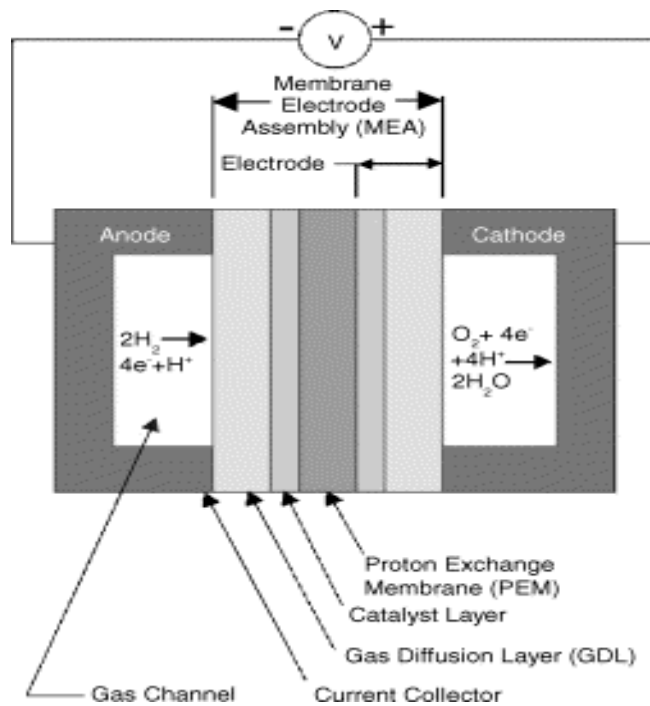


Figure 1.2. A typical polymer electrolyte fuel cell scheme [16].

PEM cells operate at a temperature of around 80°C . At this low temperature the electrochemical reactions would normally occur very slowly so they are catalysed by a thin layer of platinum on each electrode [17].

This electrode/electrolyte unit is called a membrane electrode assembly (MEA) and it is sandwiched between two field flow plates to create a fuel cell. These plates contain grooves to channel the fuel to the electrodes and also conduct electrons out of the assembly. Each cell produces around 0.7 volt, just enough power to run a light bulb, in contrast to around 300 volts needed to run a car [18]. In order to generate a higher voltage a number of individual cells are combined in series to form a structure known as a fuel cell stack.

1.4. Main PEMFC Components

There are four main components in PEMFC namely: membrane, electrodes, gas diffusion layer and bipolar plates. Proton-conducting membrane forms the heart of each cell and electrodes. Membrane combines with porous carbon including catalytic platinum to form a membrane electrode assembly (MEA). A Bipolar Plate is used to interconnect the anode of one cell to the cathode of the next. Gas diffusion layer must to be good gas diffusion properties with suitable water permeability, good electric conductivity and high endurance to the physical and chemical attacks [19].

1.4.1. Membrane

A solid proton conducting ionomer membrane is used as the electrolyte in PEM fuel cells. The electrolyte conducts protons from anode to cathode electrode and prevents mixing and direct combustion of reactants. It does not conduct the electricity. Most of PEM fuel cells utilize perfluorosulfonic acid polymer membranes, which consist of perfluorovinyl ether groups terminated with sulfonate groups incorporated onto polytetrafluoroethylene (PTFE) backbone. The most common membrane material is Nafion® [20]. Ionomer membranes for PEM fuel cells have to have high chemical and physical durability, high proton conductivity, and preferably low price. Current PFSA membranes are chemically and physically stable, but their proton conductivity depends strongly on the degree of humidification. Furthermore, best humidification is achieved by contact with liquid water, and therefore operating temperature is limited to the range where water exists in liquid form. Under very dry conditions or at temperatures above boiling point membranes lose absorbed water and conductivity drops drastically. Fully humidified, proton conductivity of common membranes can reach values from 1 to 10 S m⁻¹ [21]. Current PEMFC membrane research concentrates on two main themes, high temperature membranes and alternatives to expensive PFSA

materials, which are partially overlapping. High temperature membranes are the subject of intensive research and development efforts [22].

1.4.2. Electrode

A fuel cell electrode is essentially thin catalyst pressed between membrane and porous, electrically conductive substrate. The electrochemical reactions take place on the catalyst surface. Typically, a PEMFC electrode consists of a mixture of ionomer and catalyst that are suspended on carbon black particles. The most common catalyst in PEMFC for both oxygen reduction and hydrogen oxidation reaction is platinum. Average catalyst loading on an electrode is usually between 0.1 and 0.4 mg cm⁻² for both anode and cathode[23]. It is important to have small Pt particles with large surface area finely dispersed on the surface of the catalyst support. Typically support materials are Vulcan XC 72R by Cabot and Ketjen Carbon Black [24].

Most of research in PEMFC electrodes is focused on the cathode side. Since, kinetics of oxygen reduction reaction (ORR) in acidic environment at the cathode are relatively slow comparing hydrogen oxidation reaction, under normal operating temperatures, PEMFC electrodes should have high effective area and contain noble metal catalysts [25,26,27]. High effective area is attained by creating a highly porous three-dimensional structure, where the ionomer and catalyst are in contact with each other and accessible to the gas phase and electron conductor and to allow actual electrochemical reaction takes place on the catalyst surface. Porosity is an essential property of a high performance electrode. Pores allow transport of reactants onto three phase boundary sites and removal of reaction product water [28].

Oxygen reduction reaction is the cause of the cell potential losses. In order to minimize this fact, the electrocatalyst layer should be made reasonably thin and not only should catalyst utilization be increased but also its active sites should be enhanced [29].

1.4.3. Gas Diffusion Layer

In PEMFC, gas diffusion layer is located between the catalyst layer and bipolar plates. They also called porous transport layers have numerous functions in a PEM fuel cell [30]. Traditionally, PEMFC gas diffusion layers have been made of carbon cloth, paper or felt treated with PTFE or similar fluorocarbon to increase hydrophobicity, i.e. to ensure that water does not fill all the pores. Many gas diffusion layers feature a microporous layer of carbon black and PTFE on one or both sides to improve water management properties [31]. If the electrodes are manufactured onto the gas diffusion layer, Pt/C catalyst is bound onto the microporous layer or directly onto the gas diffusion layer substrate by ionomer or ionomer/PTFE solution. They act as a conduit for reactant species, reaction products, electric current and heat. Furthermore, they provide mechanical support for the MEA, ensuring a sufficient electrical and thermal contact between the MEA and the gas diffusion layer under the flow channels. The porous nature of the gas diffusion materials provides the reactants access to the parts of the electrodes that are under the flow channel ridges, and a passage for reaction product water from the electrode to the flow channel. Reactant transport is usually driven by diffusion and in some cases by convection and water removal by capillary action. Electric current passes through the gas diffusion layers when electrons travel from the cathode to the anode electrode via an external circuit, and heat produced in the cathode reaction leaves the MEA mainly by conduction through the gas diffusion layer [32]. Porous transport layers are a critical component in cell water management, and experiments and modeling have shown that majority of mass transfer losses occur due to limited oxygen diffusion through the cathode side gas diffusion layer, especially when liquid water is present [33].

1.4.4. Bipolar Plate

Bipolar plates are necessary for multicell configurations they are used to connect the anode of one cell and the cathode of the adjacent cell by electrically. Thus, they must be electrically conductive. At the same time, they provide structured surfaces to guide reaction gases and products as they enter or leave the cell. One bipolar plate should meet also upcoming qualifications: high chemical resistance, high mechanical stability at low thickness, heat conductivity and corrosion resistance. In general, bipolar plates are divided into two categories: graphite based; graphite-composite, carbon-composite bipolar plates and metallic plates [7].

1.5. Motivation

There are mainly two problems related with electrodes in the PEMFC that should be overcome: The price of the electrode materials, and efficiency of the catalysts. Loading of 0.1 to 0.4 mg Pt/cm² are typically found in PEMFC electrodes but it is still around 100\$/kW, so it is not economically superior [34]. In addition, the oxygen reduction reaction at the cathode is primarily the cause of the cell voltage losses, catalyst utilization become crucial part at MEA. Moreover, conventional supports such as carbon black and Vulcan XC are often isolating each other in MEA [35], resulting poor electron transfer. Therefore, more active, better structured and at the same time cheaper catalyst-supporter systems are required. Electrospun Pt or Pd nanoparticles including carbon nanofibers have strong potential to solve many of these challenges.

1.6. Electrospinning

Electrospinning is a process that produces nanofibers through an electrically charged jet of polymer solution or polymer melt. The first electrospinning experimental set up was patented by Formhals in 1934 [36]. In the electrospinning process a high voltage is used to create an electrically charged jet of polymer solution or melt, which dries or solidifies to leave a polymer fiber. One electrode is placed into the spinning solution/melt and the other attached to a collector. Electric field is subjected to the end of a capillary tube that contains the polymer fluid held by its surface tension. This induces a charge on the surface of the liquid. Mutual charge repulsion causes a force directly opposite to the surface tension [37]. As the intensity of the electric field is increased, the hemispherical surface of the fluid at the tip of the capillary tube elongates to form a conical shape known as the Taylor cone. With increasing field, a critical value is attained when the repulsive electrostatic force overcomes the surface tension and a charged jet of fluid is ejected from the tip of the Taylor cone. The discharged polymer solution jet undergoes a whipping process wherein the solvent evaporates, leaving behind a charged polymer fiber, which lays itself randomly on a grounded collecting metal screen. In the case of the melt the discharged jet solidifies when it travels in the air and is collected on the grounded metal screen. A schematic diagram of the electrospinning is shown below, in figure 1.3.

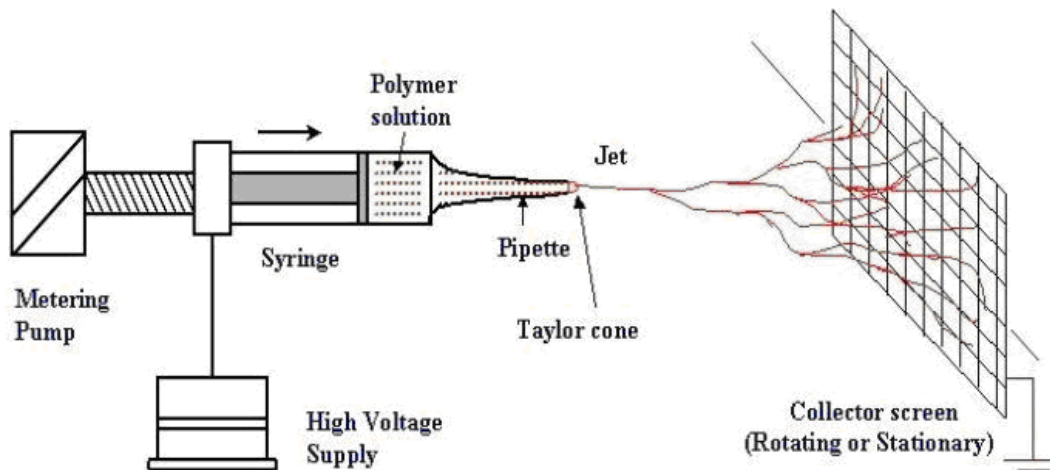


Figure 1.3. A schematic diagram of electrospinning setup

The polymer solution or melt is contained in a glass tube, usually a pipette that is connected to a syringe like apparatus. A metering pump attached to the plunger of the syringe generates a constant pressure and flow of the fluid through the pipette. The driving force is provided by a high voltage source through a wire immersed in the solution. The high voltage source can generate up to 30 kV, and the setup can be run on either positive or negative polarity. Adjusting the flow of the fluid and the magnitude of the electric field controls the spinning rate [38].

The electrospinning process consists of a DC power supply, a pipette to hold polymer solution and grounded metal collector. Suitable solvent should be necessary for dissolving polymer and viscosity. Also surface tension of the solvent must neither be too large to prevent jet from forming nor be too small to allow the solution to drain freely from the pipette. The DC power supply should be adequate to overcome the surface tension of the solution to form jet. The gap between the metal collector and the pipette should not be too small to create spark, should be large enough for the solvent to evaporate in time for the fibers to form. In short screen distance, applied potential, flow rate and polymer solution concentration are the main parameters that affect the fiber diameters. In figure 1.4 summarizes the process parameters that influence the diameter of the fibers [39].

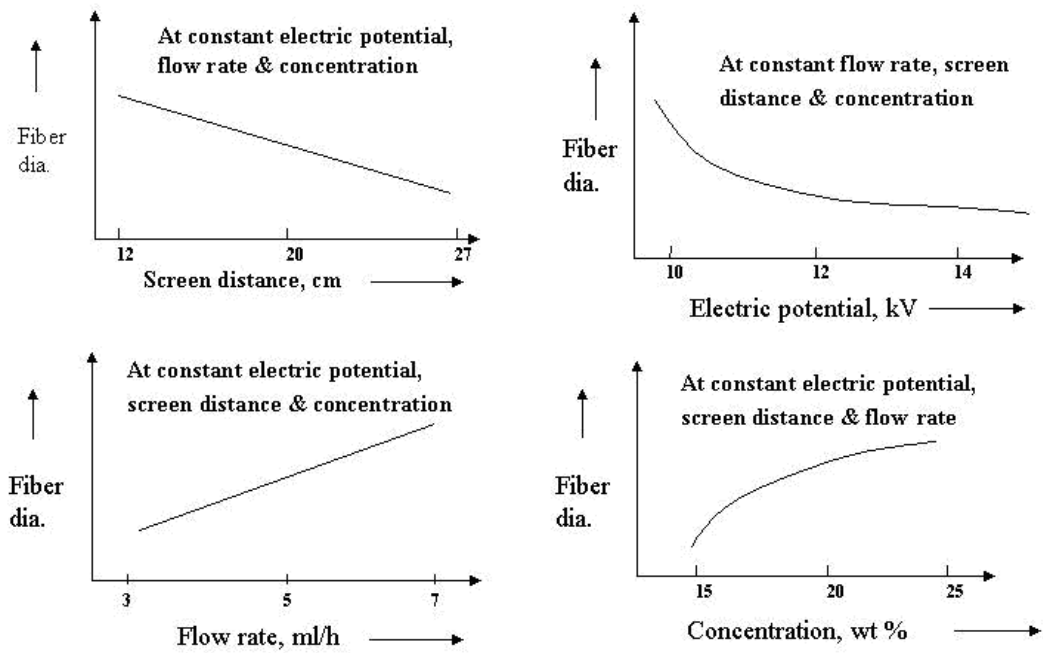


Figure 1.4. Electrospinning Process Parameters

An important characteristic of electrospinning is the ability to make carbon fibers with diameters in the range of nanometers to a few microns. By means of electrospinning, polymers and polymeric nanofibers and composites can be produced directly while ceramics and carbon nanotubes require further processing of the electrospun fibers. Consequently these fibers have a large surface area per unit mass so that nanowoven fabrics of these nanofibers collected on a screen can be used for example, for filtration of submicron particles in separation industries and biomedical applications such as wound dressing in medical industry, tissue engineering scaffolds and artificial blood vessels. Highly porous electrospun fibers with high surface area are desirable for catalyst support structures and electrode materials [40].

CHAPTER 2

2. EXPERIMENTAL

In this chapter, the experimental techniques for preparation and characterization of carbon nanofibers were explained in details. It was divided into, polymer synthesis, electrospinning, reduction, heat treatments and characterizations. Materials, synthesis methods and characterization were described in following sections.

2.1. Materials

Monomers, Acrylonitrile (MW = 53.1 g/mol), n-vinylpyrrolidone (MW = 111 g/mol), acrylic acid (MW = 72.06 g/mol) and the initiator, 2,2'-azo-bis(isobutyronitrile) (AIBN MW = 164.21 g/mol), were supplied from Sigma Aldrich. N,N-dimethyl formamide (DMF, MW = 73.09 g/mol) were purchased from Merck.

Palladium (II) chloride (PdCl_2 , MW = 177.33 g/mol, 99.9 % metal basis) and platinum (II) chloride (PtCl_2 , MW = 265.99 g/mol, 99.9 % metal basis) were obtained from Alfa Aesar. Sodium borohydride (NaBH_4 , MW = 37.83 g/mol) was purchased by Alfa Chemicals, while hydrazine (N_2H_4 , MW = 32.05 g/mol) was taken from Merck.

Nafion (Perfluorinated ion-exchange resin 20 % wt, solution of aliphatic alcohols / water mix) was supplied from Aldrich.

2.2. The synthesis of polyacrylonitrile copolymers

All monomers were purified before the reactions by conventional methods; recrystallization, vacuum distillation and passing through a column where needed. The solution copolymerization of acrylonitrile (AN) with different monomers was accomplished in N,N-dimethylformamide (DMF) at 80⁰C for 24 hours. Monomer feed ratios at the solutions were selected according to their reactivities to achieve the intended composition in the final polymer backbone composition. 2,2'-azobis(isobutyronitrile) (AIBN) was used as radical initiator. The resulting product was precipitated in water and dried in vacuum oven at 70 ⁰C until their weight become stable.

2.3. Electrospinning of metal containing polymer solutions

The polymer - metal solutions were prepared via combining the synthesized polyacrylonitrile copolymers, DMF with (10-20% by weight) and metal salt PdCl₂ or PtCl₂ with the metal ratio of 2-20% by weight. First, the polymer was dissolved in solvent, and then metal salt was added. To dissolve metal salt into solution two drops of concentrated HCl was added and solutions were continuously stirred until the metal salt completely dissolved.

In order to investigate the effects of some of the key process parameters on fiber morphology, electrospinning of the polymers was conducted at different conditions. The

parameters studied were concentration, capillary- plate distance and applied voltage. Volume percentage of DMF in the solvent mixture (viscosity), the applied voltage and the capillary tip to metal collector distance were changed in the process of the electrospinning.

Home made electrospinning set up and metal collector was shown in picture 2.1. and 2.2.

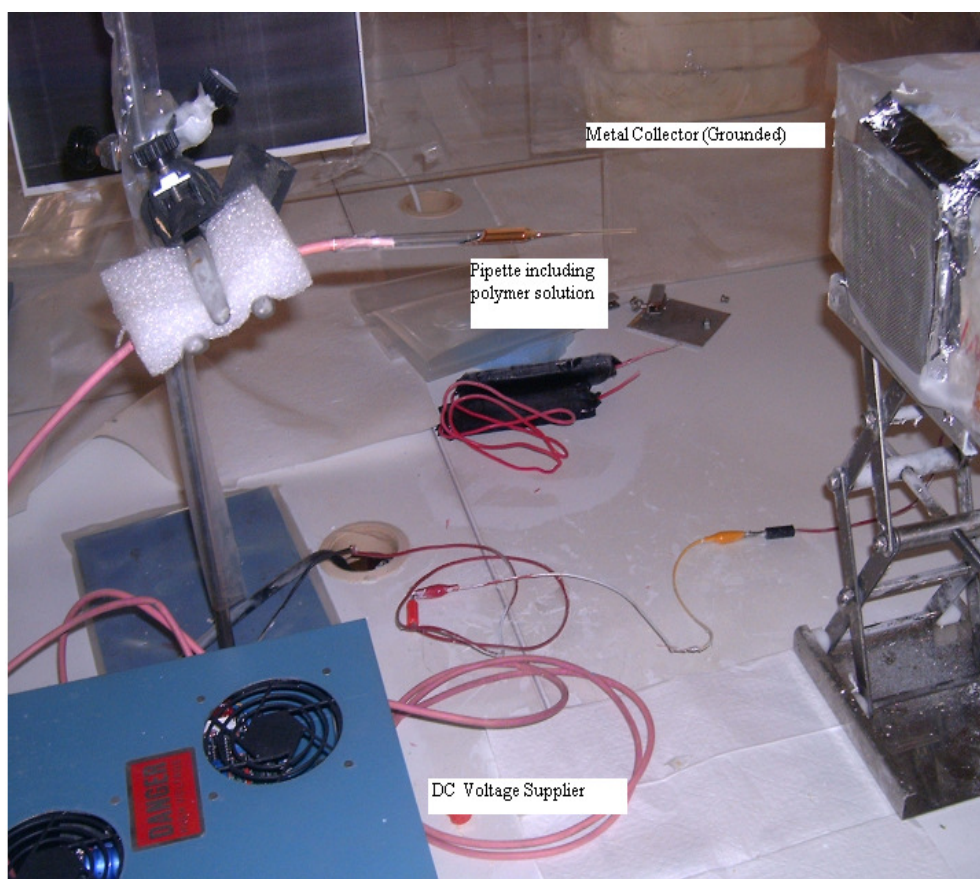


Figure 2.1. Picture of typical home-made electrospinning setup

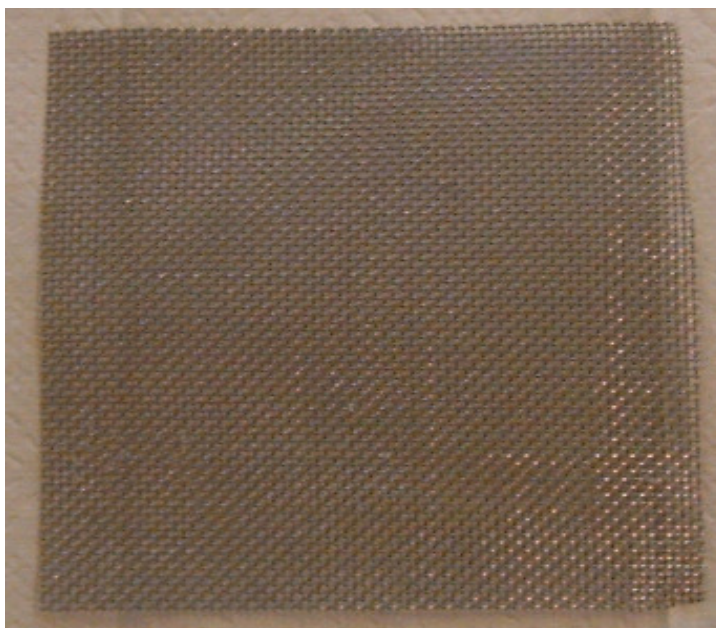


Figure 2.2. Picture of 10 X 10 cm² aluminum mesh metal collector

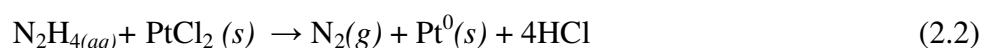
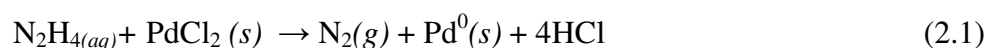
At a typical electrospinning experiment, 10kV voltage difference was applied to 10 cm x10 cm grounding collector which was 15 cm apart from the electrospun solution. Figure 2.1 showed a typical home made electrospinning set up. To increase the strength of electrospun fiber, 10 cm x10 cm aluminium mesh collector was used. A summary of the electrospinning conditions were illustrated in table 2.1.

Parameter	Range
Applied Voltage	10-20 kV
Tip to collector distance	10-20cm
Concentration of polymer	5-20 wt%
Concentration of metal	5-20 wt%

Table 2.1. Summary of the electrospinning working condition

2.4 The reduction of metals

In order to get electro-active metal particles, the oxidation state of the metals should be zero. PdCl₂ or PtCl₂ were used as metal precursor. Two strong reducing agent sodium borohydrur and hydrazine were tried with different molarities. Electrospun fibers were put on diluted or concentrate reducing agents for 1hour, 2 hours and 24 hours. Since it yielded smaller metal particle, dilute hydrazine was chosen for 1 hour reducing treatment for the metals. (Equations 2.1 and 2.2)



After that, the fiber mat was washed with distilled water and kept vacuum furnace for 24 hours at 40⁰C.

2.5 Heat Treatments

Heat treatments of polymer fibers consisted of two steps: Stabilization and carbonization (pyrolysis). The first heat treatment is a stabilization step which oxidizes and stabilizes the polymers before carbonization step [41]. The stabilization step occurred in air atmosphere and consisted of raising the temperature from 25⁰C to 200⁰C at 5⁰C per minute and holding for 30 minutes. The second heat treatment was carbonization which followed by stabilization step. The process occurred in nitrogen atmosphere and began from 200⁰C to 600, 800, 1000 and 1200⁰C with various heating rates as, 5, 20 and 40⁰C per minute. Heat treatments were conducted in Netzsch 449 C

Jupiter TGA instrument which has $0,1^{\circ}\text{C}$ sensitivity. In Figure 2.2 a sample heat treatment process was illustrated.

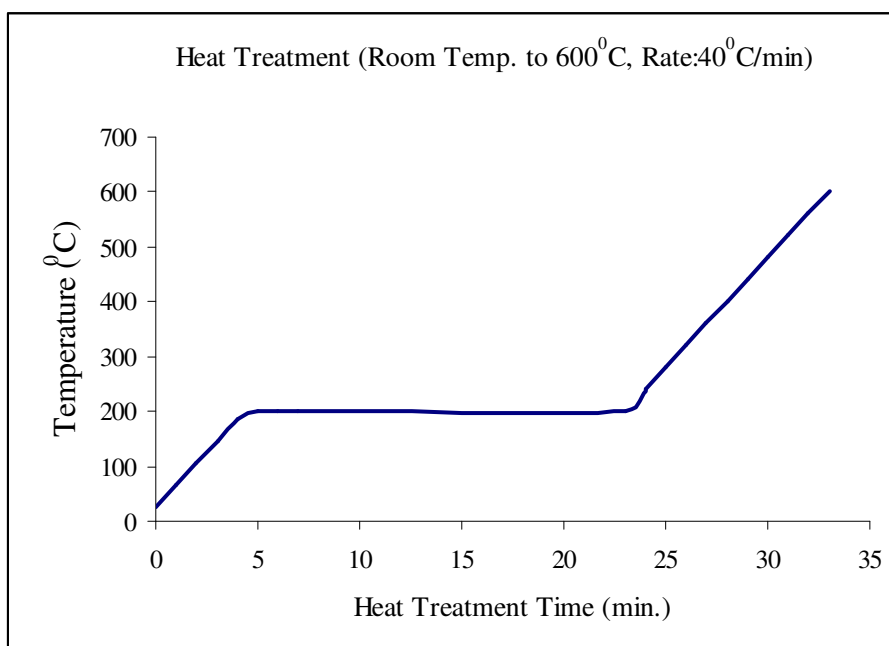


Figure 2.3. Heat treatment ramp rate: $40^{\circ}\text{C}/\text{min}$

2.6 Characterization of polyacrylonitrile copolymers

Structural characterizations of polyacrylonitrile copolymers were carried out with FT-IR spectroscopy and ^1H NMR spectroscopy. Bruker Equinox 55 FT-IR and 500 MHz Varian Inova were used as instruments.

In order to determine the glass transition temperature (T_g) and the melting temperature (T_m) of polyacrylonitrile copolymers thermal analysis was conducted via Differential Scanning Calorimetry (DSC, 204 Phoenix, Netzsch) at N_2/LN_2 atmosphere and Netzsch 449 C Jupiter Thermal Gravimetric Analyzer (TGA) in both nitrogen and oxygen atmosphere.

2.7 Characterization of Fibers

Characterization of fibers was examined via optical microscopy, x-ray diffractometer, scanning electron microscopy and tunneling electron microscopy.

2.7.1 Optical Microscopy

Fiber characterization began with electrospinning. During electrospinning, optical microscopy (Nikon Eclipse ME600) was used to control fiber formation according to pipette to collector distance and applied voltage.

2.7.2 X-Ray Diffraction (XRD)

Powder X-ray diffraction (XRD) is a powerful and useful technique that allows for rapid, non-destructive analysis without the need for extensive sample preparation.

XRD patterns showed peaks at the specific angles for crystalline materials. Moreover, peak patterns are specific for individual metals, ceramics and etc. Resulting peaks were used for determining average crystal metal size via Debye- Scherer formula [42]:

$$L = \frac{0,9 \times \lambda_{K\alpha}}{B_{(2\theta)} \cos \theta_B}$$

Figure 2.4 Debye Scherer Formula

where L was the average crystal size, B was the full width half maximum (FWHM) of the peak, θ was the diffraction angle and λ was the wavelength of the x-rays, that was fixed at 1.5406 Å for Cu-K $_{\alpha}$

Crystal structure and size of the nano metalparticles were studied with x-ray powder diffractometer (Bruker AXS-D8) after reduction and heat treatment steps. The measurements were performed in the 2θ range of 30° - 45° and 30° - 90° at 40 kV and 40 mA, using Cu-K $_{\alpha}$ radiation and in all measurements, the step size was 0.03° . A typical full scan ranged from 30° to 90° . 30° - 45° 2θ range was used for the analysis of (111) crystal peak that starting 39,7 to 40,8 2θ . FWHM was obtained directly from the instrument software.

2.7.3 Scanning Electron Microscopy (SEM)

Fiber morphologies, metal nanoparticle distributions and sizes (up to 5 nm) were investigated by scanning electron microscope (SEM) analyses (Supra 35VP Field Emission SEM, Leo). Although, it was not necessary for conductive carbon fibers, the samples that were not carbonized or carbonized below 850°C were coated carbon under Ar atmosphere with an EMITECH K950X.

2.7.4 Tunneling Electron Microscopy (TEM)

The size of the nanoparticles can be analyzed via TEM that allowed much higher resolution than the SEM. Jeol 2100 and FEI Super Twin FE-TEM Tunneling Electron Microscopy was used (TEM) for particles that was less than 10 nanometers.

2.8 Cyclic Voltammetry (CV)

Cyclic Voltammetry is a very sensitive and fast electrochemical technique that is frequently used in fuel cell research in order to qualify and quantify electrochemical performance of the the catalysts in both anode and cathode sides of a polymer electrolyte membrane fuel cells [43].

In a typical cyclic voltammetry experiment, a specific voltage is applied to a working electrode in solution current response is measured and plotted versus applied voltage to give cyclic voltammogram. Furthermore, both anodic and cathodic voltage and currents are determined via a cyclic voltammogram. It starts with an initial potential value up to defined limited value. At this potential, the direction of the limited value is reversed and same potential is scanned in the opposite direction up to initial potential value. Materials formed by oxidation on the first (forward) scan can be reduced on the second (reverse) scan. Usually, more than one cycle is carried out and scan rates can be varried. The shape of the cyclic voltammogram is highly dependent on the rates of the electron transfer, mass transfer and chemical reactions occurring at the electrode surfaces [44]. A typical cyclic voltammogram was illustrated in figure 2.4.

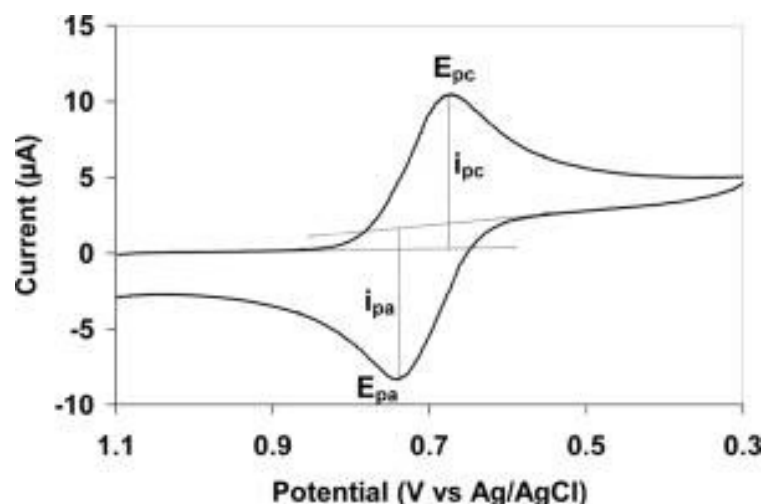


Figure 2.5. A typical cyclic voltammogram.

Using cyclic voltammograms with suitable potential windows and sweep rates, reproducible surface conditions for most metals can be obtained. In order to investigate the catalytical behaviors of the metals via cyclic voltammograms, three –electrode method is used widely. It consists of a working electrode, reference electrode and counter electrode (also called auxiliary electrode). To ensure sufficient conductivity electrolyte is also added to the conventional three electrode cells [44]. In the cell, the electrochemical reactions take place on the working electrode. Silver, gold, platinum and glassy carbon electrodes are used commonly as a working electrode. Reference electrodes that are used in the cell should be stable and have well-known electrode potential so that working electrode potential can be measured. Some of the frequently used reference electrodes are standard hydrogen electrode, saturated calomel electrode, copper-copper (II) sulfate electrode.

In a three-electrode cell, a counter electrode, also called an auxiliary electrode, is used to make a connection to the electrolyte so that a current can be applied to the working electrode and to ensure that current does not run through the reference electrode. The counter electrode is usually made of an inert material, such as a noble metal or graphite, to keep it from dissolving. Commonly, a platinum wire electrode is used as a counter electrode in three- electrode cells [44]. Glassy carbon electrode was used as working electrode while platinum wire was the counter electrode. Saturated

calomel electrode (Hg,Hg₂Cl₂) was selected as reference electrode. 0,5M H₂SO₄ solution was served as electrolyte.

2.8.1 Electrochemical Testing Setup

In all experiments, polished glassy carbon electrode was used as working electrode while platinum wire was the counter electrode. Saturated calomel electrode (Hg,Hg₂Cl₂) was selected as reference electrode. 0,5M H₂SO₄ solution was served as electrolyte.

Gamry Instruments Framework and Gamry Echem Analyst programs were used to measure and analyze the electrochemical performance of the catalysts on the electrode. Nitrogen gas was bubbled for 25 minutes through the cell to remove excess amount of the oxygen in the electrolyte prior to each measurements. In figure 2.3 a picture of typical three- electrode working cell was shown.

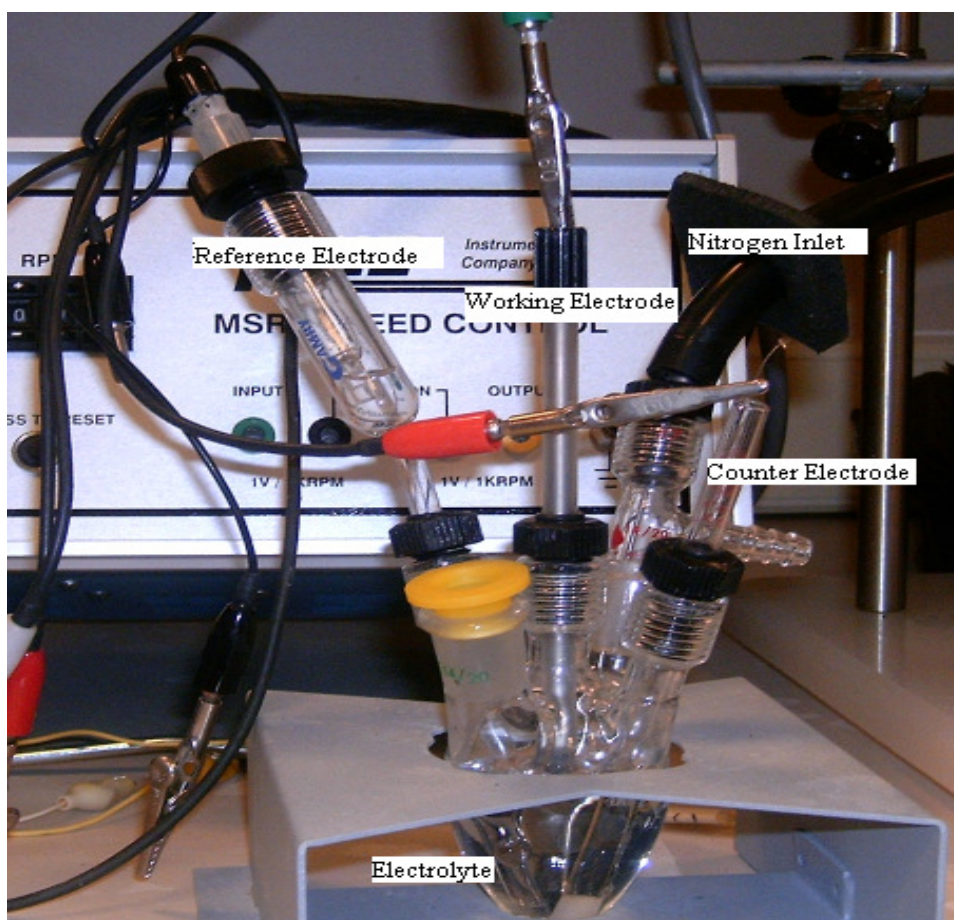


Figure 2.6. Three electrode electrochemical working cell

2.8.2. Electrode Preparation

The electrode solution was prepared via mixing 4 mg of Pd or Pt nano catalysts including carbon fibers, 0.5 ml of Nafion (Aldrich, 20 wt%) , 0.25 ml of isopropyl alcohol and 2 ml of distilled water. The heterogeneous mixture was sonicated until homogenous milky solution was obtained. 20 μ l of catalyst ink was dropped onto 0.3 cm diameter of glassy carbon electrode. Catalyst amount was set to 0.4 mg/cm². Glassy carbon electrode was polished by Al₂O₃ prior to electrode preparation. Then, the electrode was left to air dry for 30 minutes.

CHAPTER 3

3. RESULTS AND DISCUSSION

3.1 The synthesis of Polyacrylonitrile Copolymers via Solution Polymerization

Among the various polymerization techniques used in the production of acrylonitrile polymers, solution polymerization is one of the most popular ones [45]. The advantage of solution polymerization over the other techniques is that the polymer solution can be converted directly to the spinning dope in the process of fiber production. [46]

In this study, acrylonitrile was copolymerized with n-vinyl pyrrolidone, and acrylic acid via solution polymerization. The chemical structures of the copolymers were illustrated in figure 3.1

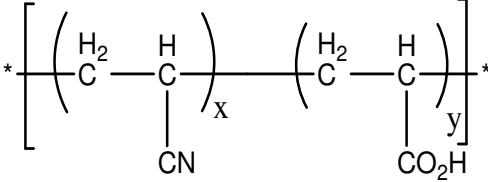
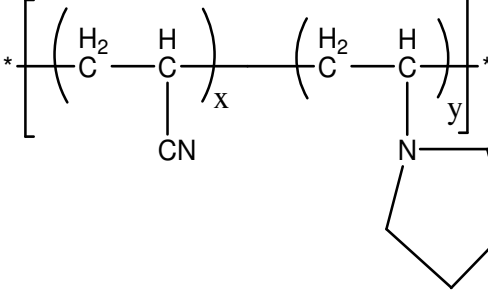
Copolymer	Chemical Structure
P(AN-co-AA) Poly(acrylonitrile-co-acrylic acid)	
P(AN-co-VPYR) Poly(acrylonitrile-co-n-vinyl pyrolidone)	

Figure 3.1 Chemical Structures of Copolymers

The ratios of the copolymers were set as 5%, 10 % and 20 % in each polymer. Structural characterizations of copolymers were examined via ^1H NMR and FT-IR analysis while the thermal characterizations were carried out by DSC and STA.

3.2 Structural Characterization

3.2.1. NMR Characterizations

The molecular structures and chemical compositions of polymers were determined by NMR spectroscopy which is widely used technique for determining the structure of organic compounds and polymers [47]. In this study ^1H NMR spectrums of the polymers were obtained in CDCl_3 . In addition, reactivity ratios of monomers were

calculated by NMR results. ^1H NMR spectrums of P(AN- co- VPYR) and P(AN- co-AA) were shown in figure 3.1.2 and 3.1.3.

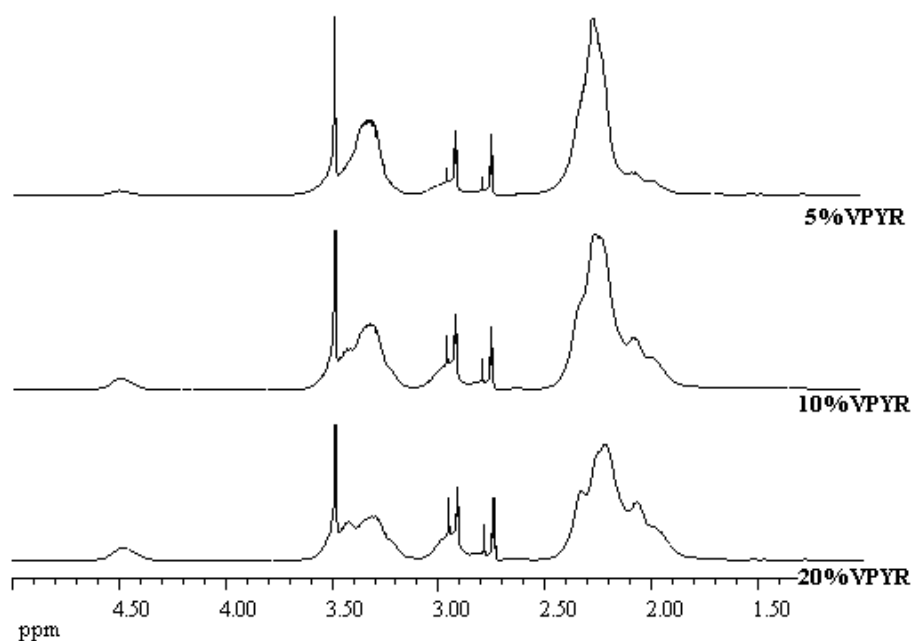


Figure 3.2. H-NMR of P(AN co VPYR)

^1H NMR spectrum was fully representative that the reactions occurred successfully. The signals were assigned as shown in figure 3.1.2 [48, 49]. The characteristic proton peaks for P(AN co VPYR) in ^1H -NMR (recorded in CDCl_3) were δ 4.50 ppm (-CH₂-CHN-CH₂-), δ 3.3 ppm (-CH₂-CHCN-CH₂-), δ 2.9 ppm (-N-CH₂-CH₂-), 2.2 ppm (-CH-CH₂-CH-).

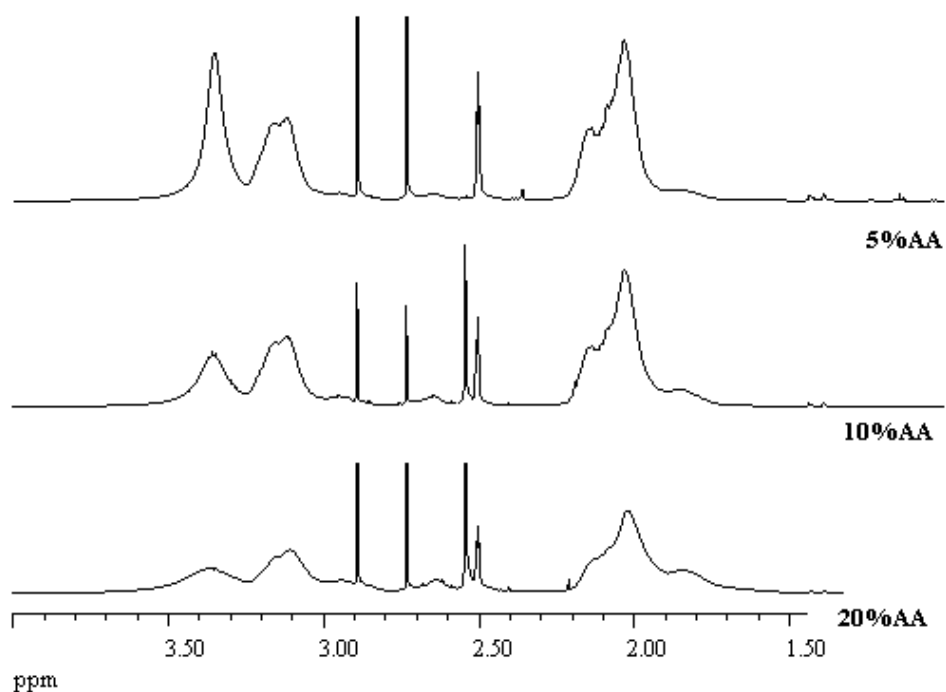


Figure 3.3. H-NMR of P(AN co AA)

Characteristic proton peaks for P(AN co AA) was δ 2.03 ppm CH_2 and δ 3.12 ppm CH that were again similar to the assignment of Bajaj *et al* [50].

The comonomer ratios in copolymers were obtained by the integral analysis of H-NMR spectrum. Since feed ratios also are known, the reactivity ratios can be calculated from Mayo-Lewis equation [51]. It was found that 0,51/3,84 and 0,46/0,06 for P(AN-co-AA) and P(AN-co-VPYR) respectively. According to Mayo-Lewis equation results suggested that, P(AN-co-AA) was a block copolymer. Although highest reactivity ratio of AA leaded to homopolymerization, reactivity ratio of AN allowed to form block copolymer. Since, both values of reactivity ratios in P(AN-co-VPYR) approached to zero, monomers could not react in homopolymerization and result was an alternating copolymer.

3.2.2. FT-IR Characterizations of P(AN-co-VPYR)

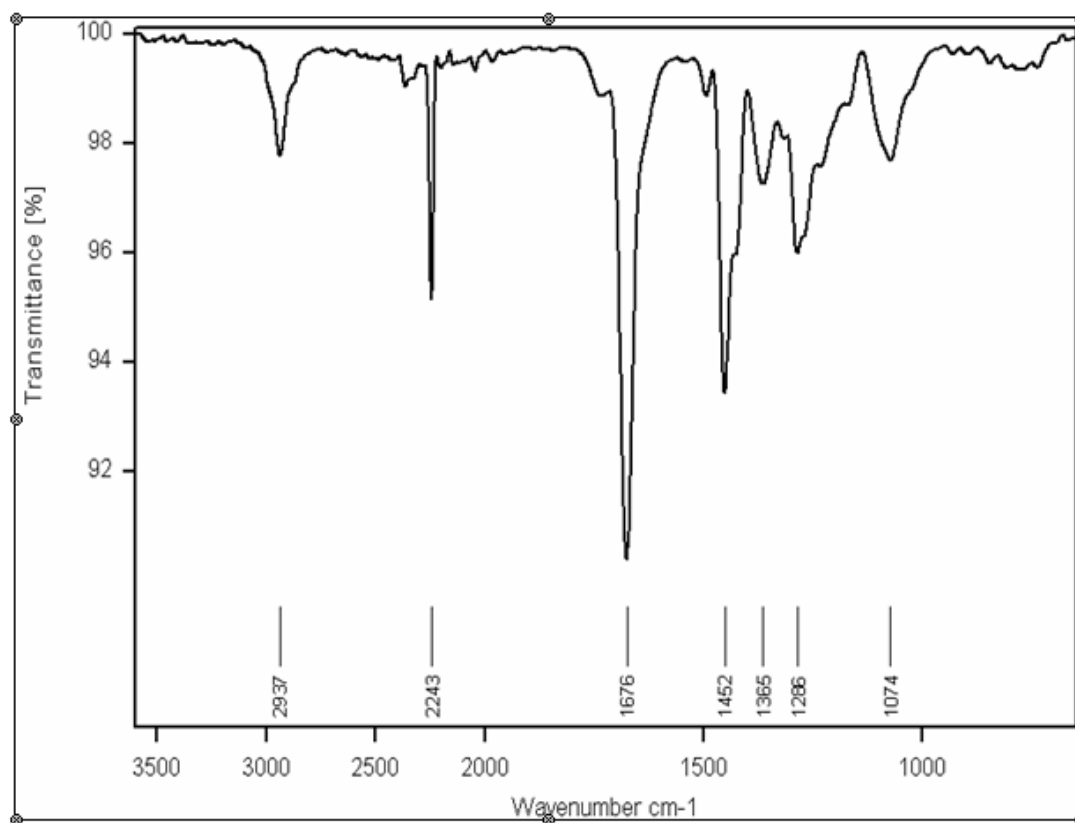


Figure 3.4. FT-IR of P (AN-co- 5%VPYR)

FT-IR spectrum (Figure3-4) analysis confirmed the NMR results for P(AN-co-5%VPYR) and showed the characteristic vibration of -CN at 2243 cm^{-1} . In addition, strong carbonyl peak at 1676 cm^{-1} confirmed the pyrrolidinone chain on the backbone. The absorption at 1286 cm^{-1} due to the stretching vibration of the C–N bond was also observed.

3.3. Thermal Characterization

Thermal analysis of polymers was achieved by Differential Scanning Calorimetry (DSC) and Simultaneous Thermal Analysis (STA). From the second endotherm of DSC analysis, the glass transition temperature (T_g) of each polymers was measured under nitrogen atmosphere and $10^{\circ}\text{C}/\text{min}$ ramp rate and the first decomposition temperature (T_m) was investigated by STA.

In figure 3-5 and 3-6 DSC curves of P(AN-co-AA) and P(AN-co-VPYR) were sketched respectively. T_g 's for 5, 10, 20 %AA comonomers were 118.6, 117.9 and 115.2°C and T_g 's for 5, 10, 20 %VPYR were 116.3, 121.3 and 123.7°C . Glass transition temperatures were decreased as the ratios of comonomers were increased for AA comonomer while the reverse trend was obtained for VPYR comonomer.

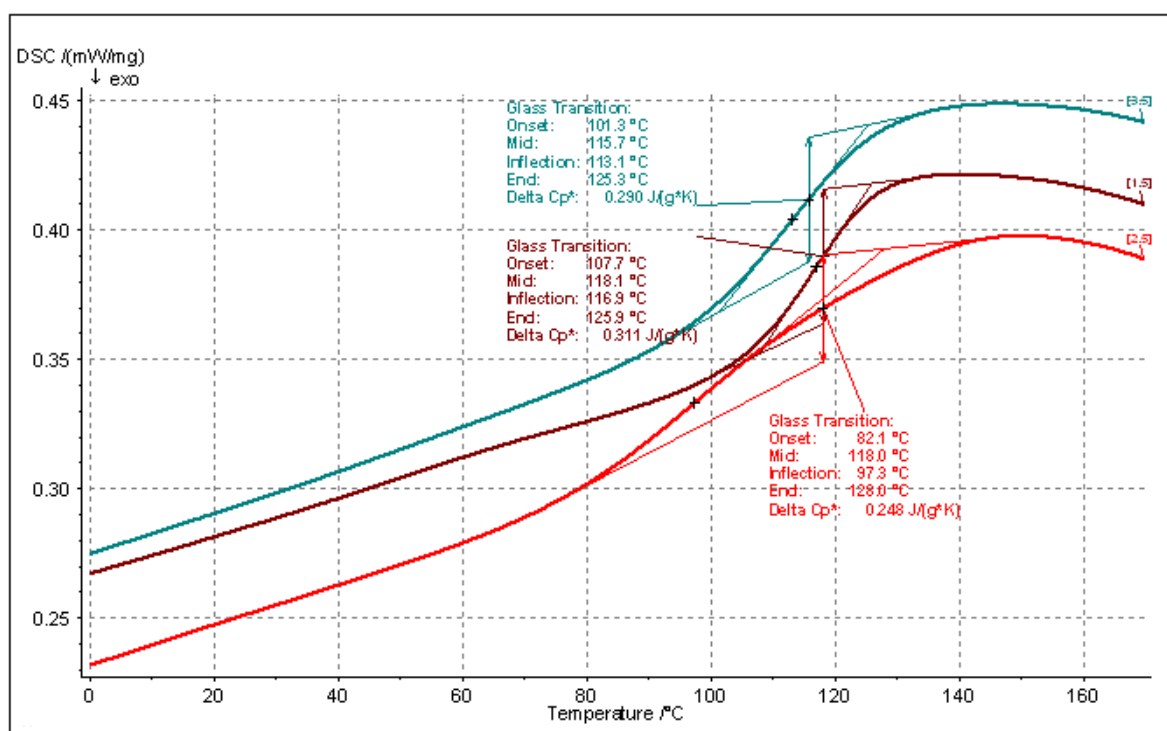


Figure 3.5. P(AN-co-AA), DSC analysis

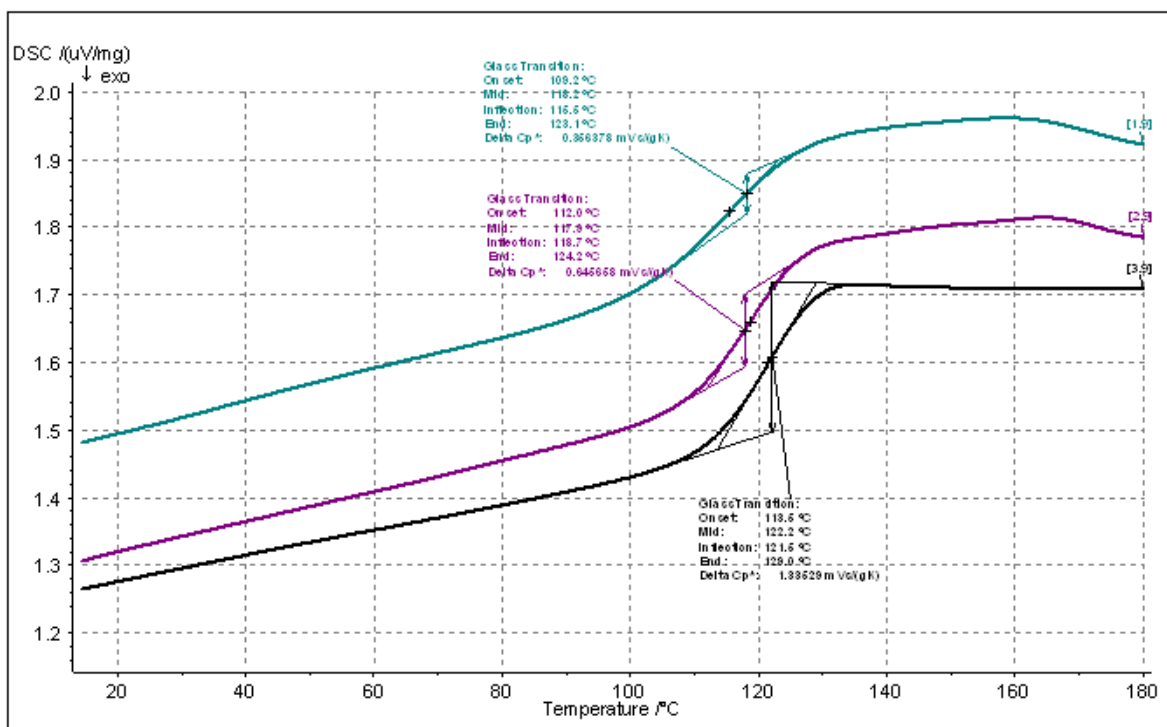


Figure 3.6. P(AN-co-VPYR), DSC analysis

Decomposition behaviors of P(AN-co-VPYR) and P(AN-co-AA) were examined by STA. As shown in the figure 3.6, decomposition beginning from about 365 $^{\circ}\text{C}$ and continues sharply to about 490 $^{\circ}\text{C}$ by the loss of 45% of total mass for P(AN-co-VPYR) to that temperature. The residual mass is around 55% at 800 $^{\circ}\text{C}$. As shown in table 3.1, increasing comonomer ratios led higher T_c value for VPYR monomer but lower T_c value for AA monomer.

Thermal analysis results confirmed that P(AN-co-VPYR) was more stable than P(AN-co-AA) during heat treatment which made it more suitable polymer during high temperature process- carbonization.

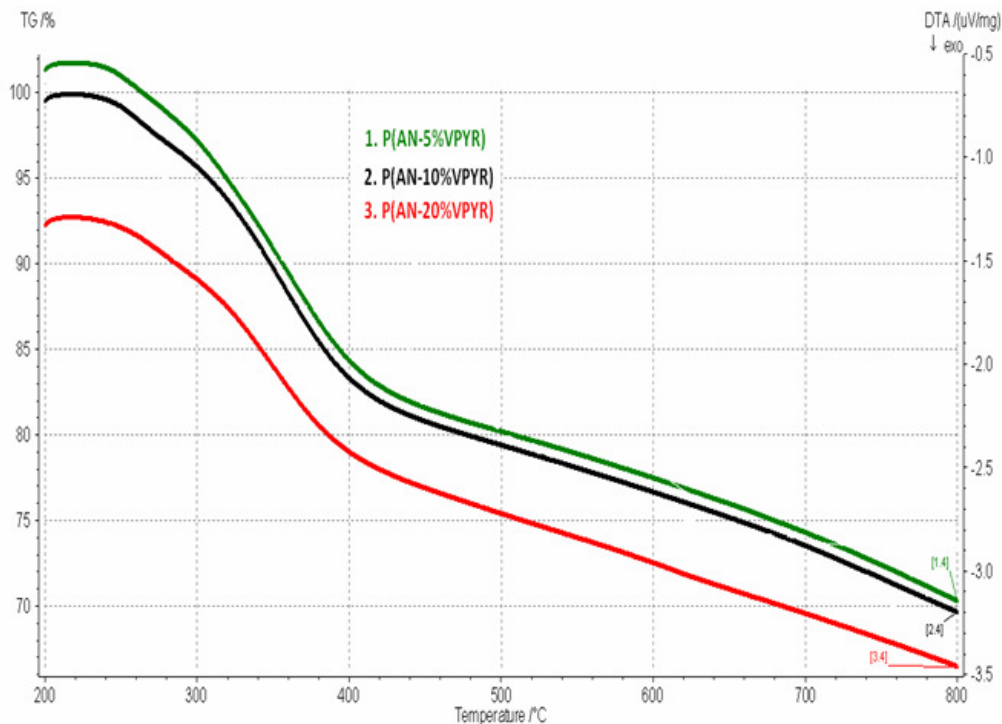


Figure 3.7. STA of P(AN-co-VPYR)

The summary of the thermal analysis and NMR results of the synthesized polymers was tabulated in table 3.5.

Copolymer	Co-monomer ratio in polymer (% mol)	Reactivity Ratio (r_1/r_2)	Product (%)	Glass Transition Temperature T_g (°C)	First Decomposition Temperature T_c (°C)
P(AN-co-AA)	5	N/AA= 0,51/3,84	5,8	118,6	259,6
	10		4,5	117,9	247,9
	20		6,2	115,2	237,7
P(AN-co-VPYR)	5	N/VPYR= 0,46/0,06	8,7	116,3	266,5
	10		1,6	121,3	283,4
	20		6,4	123,7	307,1

Table 3.1. Thermal and NMR analysis results

Both thermal and NMR results verified that VPYR comonomer was suitable candidate as a nanoparticle supporter comparing AA comonomer. It was assumed that the alternating nature of VPYR comonomer acted as surface activating agent (surfactant) for nanoparticle formation. Since it had desirable thermal stability and was an alternating copolymer, P(AN-co-VPYR) was focused in this work in details.

3.4. Electrospinning Characterization

Polymer solutions were prepared for electrospinning process to get maximum fiber density and minimum fiber diameter. The spinning parameters were optimized via applied voltage, concentration of the solution and tip to metal collector distance. During electrospinning process, different fiber diameters and morphologies were achieved due to different solution viscosities, surface tensions and conductivities.

Fiber diameters of polymers were illustrated in both table 3.2 and 3.3 In general, the diameters are changed via copolymer type and ratio, solution viscosity (concentration) and metal ratio.

As the weight percentage of metal increases for the same concentration, the fiber diameter decreases. Higher metal salt concentration enhances the solution conductivity (also viscosity) which leads thinner fiber formation [39].

Copolymer	Func. Monomer % ¹	Metal	Polymer %	Fiber Diameter (nm)
P(AN-co-AA)	5	20%Pd	19,8	400±56
			19,8	480±52
			12,5	670±71
	10		18,5	530±23
	20		19,7	140±18

Table 3.2. Fiber diameter of P(AN-co-AA). 1: Functional monomer ration in polymer, 2: Weight percentage of metal in polymer. 2: Weight percentage of polymer in solution.

Similar trends observed for Pt and Pd nanoparticles in P(AN-co-VPYR). It was well understood that, metal concentration and polymer solution viscosity (concentration) directly affected the fiber diameter. However, the fiber diameters were not depended on the comonomer ratios. Therefore, only P(AN-5%VPYR) was studied in this research.

Polymer	Functional Monomer % ¹	Metal	Metal % ²	Polymer % ³	Fiber Diameter (nm)	
P(AN-co-VPYR)	5	Pd	0,5	20	238±41	
			1	20	505±110	
			5	20	853±137	
			10	12	451±113	
			20	10	358±73	
	10		0,5	20	185±21	
			1	20	210±19	
			5	20	302±54	
	20		0,5	20	269±42	
			1	18,8	145±21	
			5	20	451±97	
	5		Pt	5	15	412±26
	10				13,5	222±21
	20				13,5	205±27

Table 3.3. Fiber diameter of P(AN-co-VPYR). 1: Functional monomer ration in polymer, 2: Weight percentage of metal in polymer. 3: Weight percentage of polymer in solution.

3.4.1 Sample SEM Images (Concentration Effect)

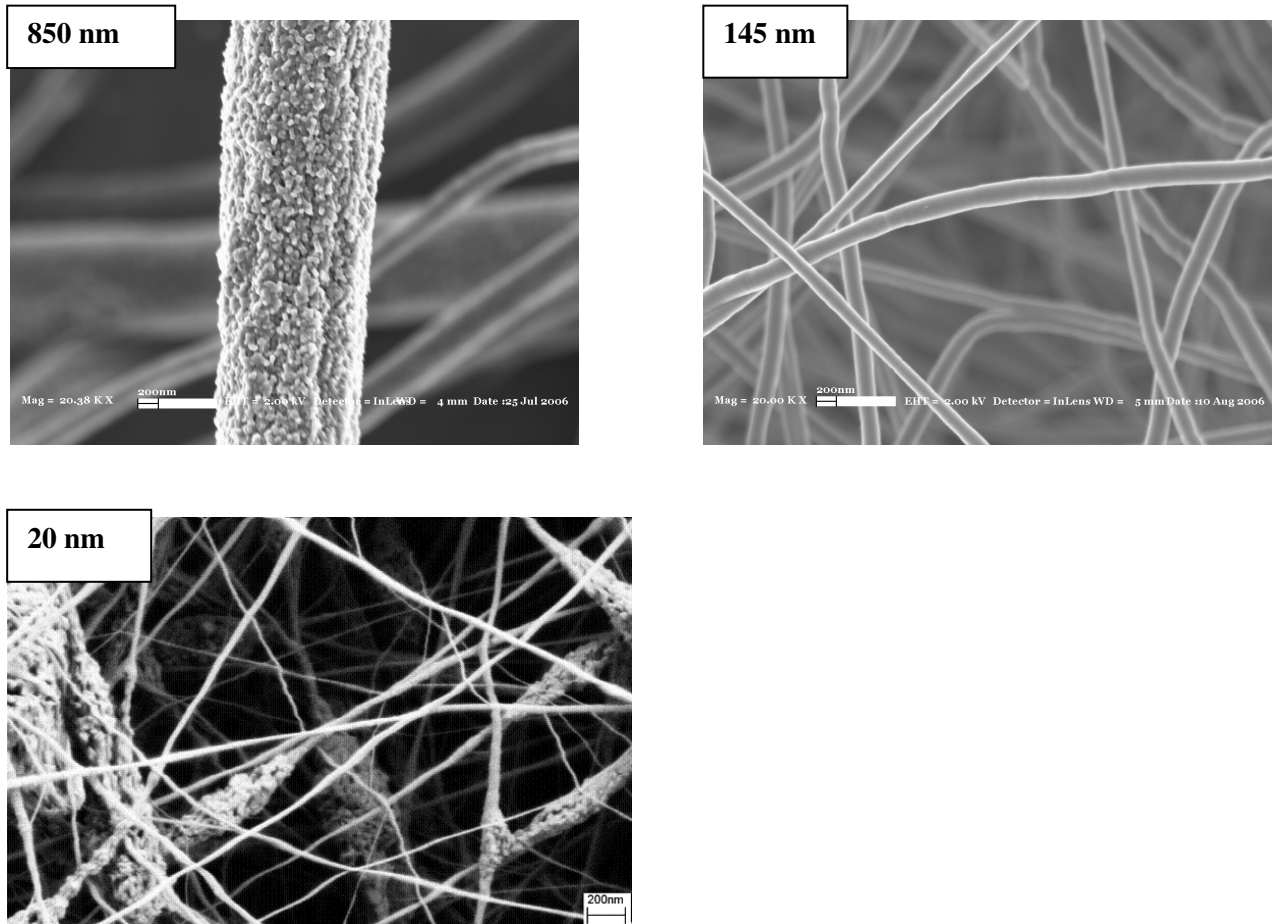


Figure 3.8. SEM images of P(AN-co- 5% VPYR) - 20, 15, 5 % weight polymer solution concentrations.

Depending on polymer solution concentrations, average fiber diameters were obtained as small as 20 nm and as large as 850 nm (Figure 3.6) it was confirmed that as the solution concentration is decreased so is the fiber diameter [40]. However, lower solution concentration, in other words, lower solution viscosity, leads the formation of beads and it is known as beads on fiber [52]. In order to get smooth connected fiber, bead formation was undesired in this research so, the polymer solution concentration was controlled in the range of 13,5- 20 %weight percentage.

3.5. Reduction characterization

After electrospinning process metal salt including fiber mat was treated with a reducing agent to get zero oxidation state of metals. According to reactions (2.x and 2y), the gas evolution and color change were observed from fiber mat and reducing agent reaction.

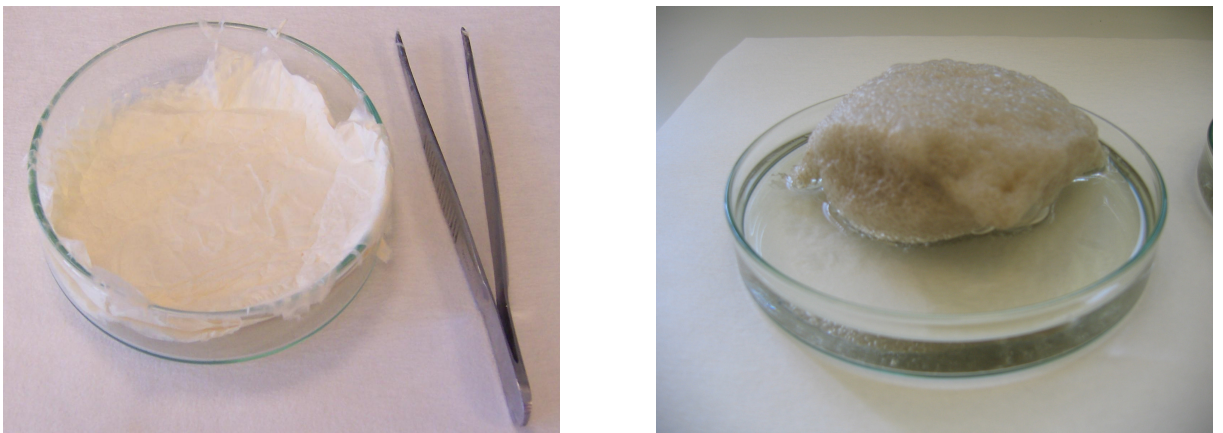


Figure 3.9. Reducing reactions: Gas evolution and color change of fiber mat before and after the reaction.

Two strong reducing agent, hydrazine and sodium borohydride were compared as mentioned in chapter 2. In the same concentration, smaller metal crystalline size obtained while dilute hydrazine was used as a reducing agent.

In figure 3.10. XRD spectrums of P(AN-co-5%VPYR)- 5%-Pd and P(AN-co-5%VPYR)- 5%-Pt were depicted. Wider peak indicates smaller particles and the crystalline size of the particles were measured quantitatively by Debye-Scherrer formula as described before in chapter 2.

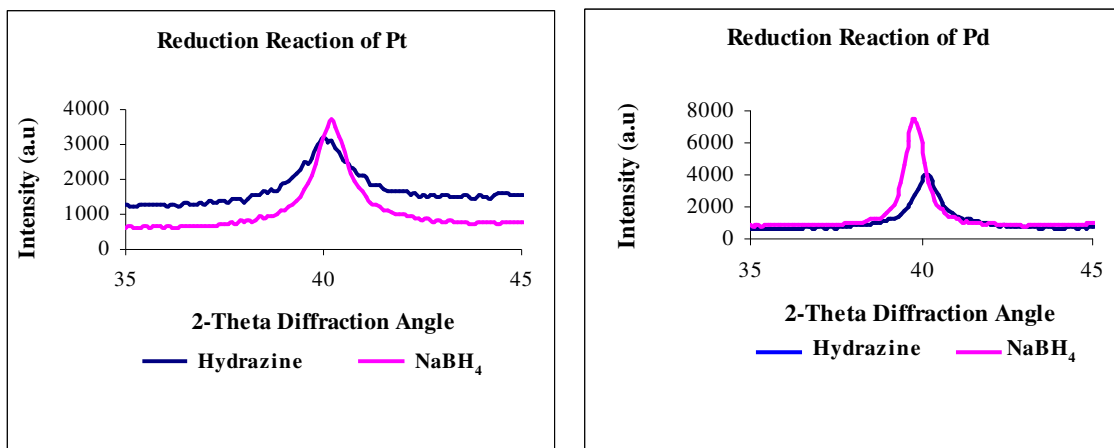


Figure 3.10. Reducing agent comparasion

Comparisons of the reduction agents were tabulated in table 3.a for the polymers P(AN-co-5%VPYR)- 5%-Pd and P(AN-co-5%VPYR)-5%-Pt. It can be seen that, using hydrazine, as reducing agent, caused smaller nanoparticle formation than NaBH₄. Moreover, concentrated reducing agent solutions enlarged the nanoparticle crystalline size. Therefore, dilute hydrazine solution was used in all reducing reactions for Pd and Pt.

Metal	Reducing Agent	Time (h)	Concentration	Fwhm (θ)	Nanoparticle crystalline size (nm)
Pd	Hydrazine	1h	Concentrated	0,325°	26,01 nm
			Diluted	0,379°	22,31 nm
	NaBH ₄		0,327°	25,85 nm	
Pt	Hydrazine	1h	Concentrated	0,721°	11,72 nm
		24h		0,625°	13,53 nm
	NaBH ₄	1h		0,457°	18,49 nm

Table 3.4. P(AN-co-5%VPYR)- 5%-Pd and P(AN-co-5%VPYR)-5%-Pt carbonized at 1000⁰C.

3.6. Carbonization Characterization

According to thermal analysis (STA and DSC) and NMR results, only Pt and Pd including P(AN-co-VPYR) polymers were carbonized, to investigate the electrochemical activities of metals.

The carbonization- heat treatment process consisted of two thermal steps. The first stage of the heat treatment involves heating the polymeric fiber to temperature of 200⁰C in air for 30 minutes at a heating rate of 5⁰C /min. The second stage of the heat treatment involves heating up to 1200⁰C in nitrogen medium at various times at a heating rate of 5⁰C, 20⁰C and 40⁰C. After cooling to room temperature, fibers and metal nanoparticle morphologies were ready to be characterized via non-destructive analytical tools such as SEM, XRD and TEM.

3.6.1. Sample SEM Images (Heat Treatment Effect)

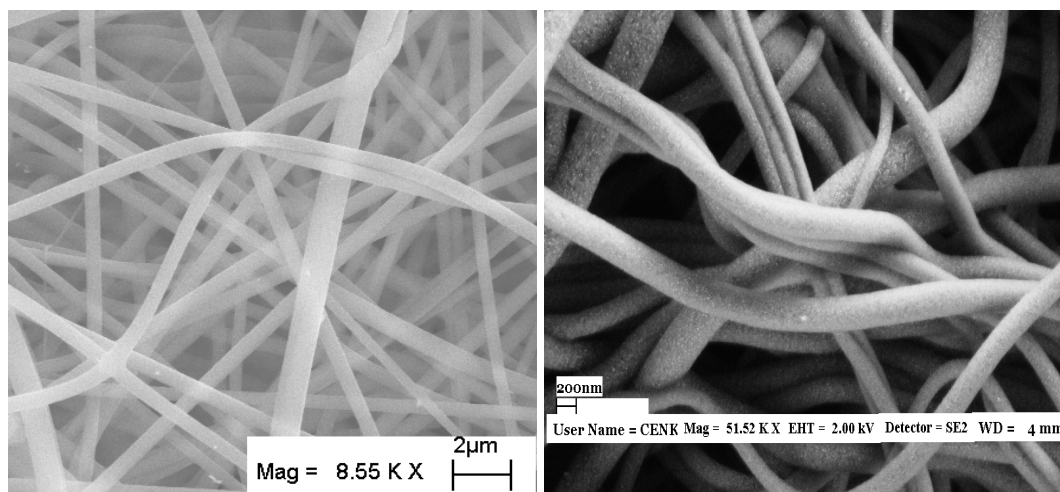


Figure 3.11. SEM images of P(AN-co-5VPYR) before and after carbonization

There were two sample SEM images in figure 3.11. before and after carbonization of the fiber. It is believed that [41] first heat treatment step from room temperature to 200⁰C in air atmosphere causes dehydrogenation forming -C=C- conjugation in the polymer backbone which makes fibers more stable. Furthermore, the first heat treatment produces heat resistance fibers that allow high temperature carbonization without melting. Carbonization process does not only produce thinner carbon fibers (figure 3.34), but also make the fibers electrically active, when the carbonization occurs at above 850⁰C. Moreover, carbonization (heat treatment process) also helps the reduction of the metal nanoparticles.

3.7 Characterization of Pt including fibers

P(AN-5%VPYR) including Pt was carbonized at 600⁰C with various concentration of Pt and different heating rate in order to understand the effects of the variables. The minimum particle size was obtained when the heating rate was 40⁰C /min for 5% weight percentage of Pt. Furthermore, higher metal concentration did not mean larger the particle (Table 3.5.). But rate and fiber diameter directly affected the particle size. It was also verified by SEM images (3.12.) the carbonization temperature was the main factor for particle size growth.

Polymer	Functional Monomer (%)	Metal	Metal (%)	Fiber Diameter (nm)	Heating Rate (°C)	Average Particle Size (nm)
VPYR	5	Pt	5	412±2 6	40	<4
			1	222±2		6,4±0,7
			0	1	20	4,3±0,6
			2	205±2 7	20	3,9±0,6
					5	4,1±0,6

Table 3.5 P(AN-5%VPYR) -%Pt carbonized at 600⁰C.

3.7.1. Sample SEM Images (Carbonization Temperature Effect)

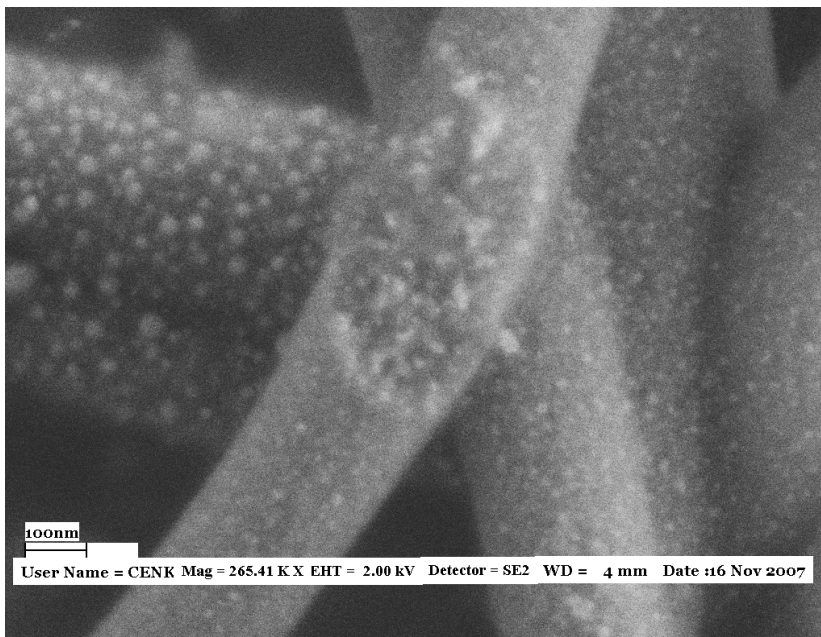
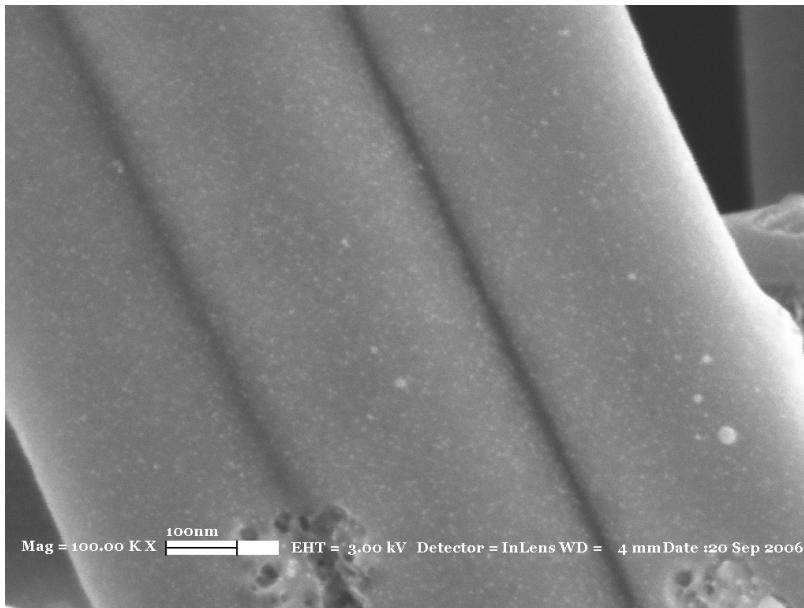


Figure 3.12. SEM Images of P(AN-co-5%VPYR)-20%Pt carbonized at 600⁰C and 1000⁰C

Particle growth was clearly seen in the sample SEM images of P(AN-co-5%VPYR)-20% in two different carbonization temperatures which confirmed the agglomeration behaviors of nanoparticles at higher temperature. Because at higher

temperature, particles that gain higher kinetic energy which enhances their vibrations and mobility. So they can move and form bigger particles.

3.8 Characterization of Pd including fibers

P(AN-co-5-VPYR) polymer included 5% Pd, the particle sizes and fiber diameters with different carbonization temperatures and various heating rate, were showed in table 3.6.

As can be understood from the table 3.6., like the Pt nanoparticles, Pd nanoparticle sizes were directly affected by carbonization temperature and heating rate. Moreover, at the same carbonization temperature and same heating rate, thinner fiber made particle size larger. It can be explained that at the thinner fiber, particle growth was faster comparing thicker fibers. Furthermore, at higher temperature, particles

Polymer	Temperature (°C)	Heating Rate (°C)	Fiber Diameter(nm)	Average Particle Size (nm)
P(AN-co-%5-VPYR), 5%Pd	600	0.1	390	5,1±0,8 38,8±11,5
P(AN-co-%5-VPYR), 5%Pd	600	1	450	4,8±1,1 32,7±6,07
P(AN-co-%5-VPYR), 5%Pd	1200	1	420	17,1±5,1
P(AN-co-%5-VPYR), 5%Pd	1200	1	415	36,6±10,2
P(AN-co-%5-VPYR), 5%Pd	1200	10	430	24,7±5,0
P(AN-co-%5-VPYR), 5%Pd	600	5	540	<4 28,6±4,9

Table 3.6 P(AN-co-5%VPYR)-5%Pd, Different carbonization temperatures and rates

In table 3.6 P(AN-co-%5-VPYR) including 5%Pd fibers were carbonized at 600⁰C and 1200⁰C with two different heating rate: 0.1 ⁰C/min and 1⁰C/min. Slower heating rate caused higher metal particle size. Moreover, there were two size distributions, among them. The average particle sizes were found 5,1nm and 39 nm for slower case, 4, 8 nm and 32, 7 nm for faster case.

3.8.1. Sample TEM Images (Heating Rate Effect)

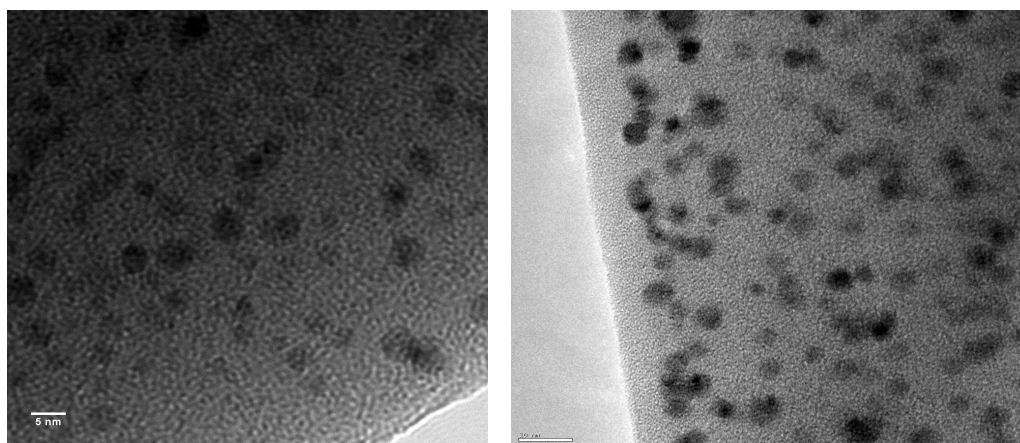


Figure 3.13. P(AN-co-%5-VPYR), 5%Pd 600C, 5 ⁰C/min heating rate Figure3d P(AN-co-%5-VPYR), 5%Pd 600C, 1 ⁰C/min heating rate

TEM analysis showed the average diameter of Pd nanoparticles was less than 4 nm for P(AN-co-%5-VPYR), 5%Pd 600C-5 ⁰C/min sample and around 6 nm for P(AN-co-%5-VPYR), 5%Pd 600C-1 ⁰C/min sample

3.9. XRD Analysis

X-Ray Diffractometer that allows fast and non-destructive analysis was used just after both reduction and carbonization step to determine the crystalline size of the nanoparticles via Debye-Scherrer formula. However, Debye-Scherrer formula has some limitations, especially when the diameter of the nanoparticles is below 4-5 nm [53]. Besides, only larger nanoparticle diameters are calculated, so results that are obtained via XRD measurements are different from SEM and TEM analysis results for nano particles.

3.9.1. XRD Analysis of Pt including fibers

After carbonization step, xrd spectrum of nanoPt particles was taken. The range between 30° and 90° crystalline directions of Pt metal was studied to get all crystalline directions. But, rather small interval between $30-50^{\circ}$ was scanned in order to calculate the crystalline size of the metals.

As shown in the figure 3.14. four different crystalline directions of Pt nanometal particles were observed that were agreed with the literature [54]. The crystalline sizes were calculated by analysis of the (111) Pt peaks using its full width half maximum (fwhm) in Debye- Scherer equation. X-ray diffractometer also confirmed the complete reduction of the metals.

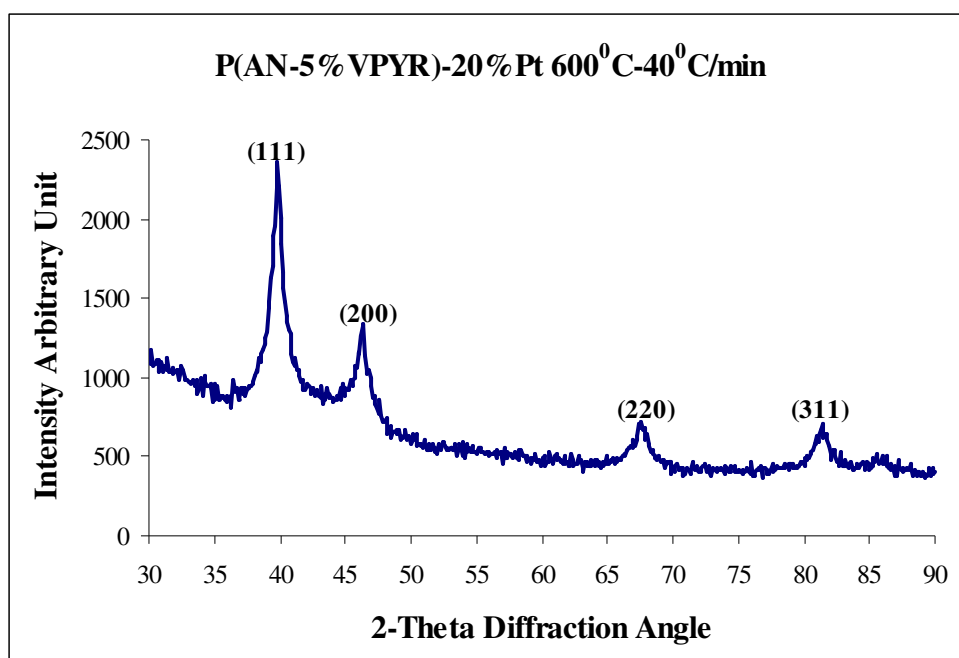


Figure 3.14. XRD Spectrum of P(AN-5%VPYR)-20%Pt carbonized at 600⁰C

The effect of different reducing agent and various concentrations was shown in figure 3.3. In addition that, without reducing process, sample polymers directly was carbonized right after the electrospinning.

XRD pattern of unreduced sample was illustrated in figure 3.5. and compared with reduced sample. Without reducing agent, the crystalline size of Pt was found as 13 nm, while the crystalline size of Pt was calculated as 9,4 nm for sample that were reduced after electrospinning. Although, the heat treatment acted as a reducing agent for metal salts, using reducing agent made the particles smaller.

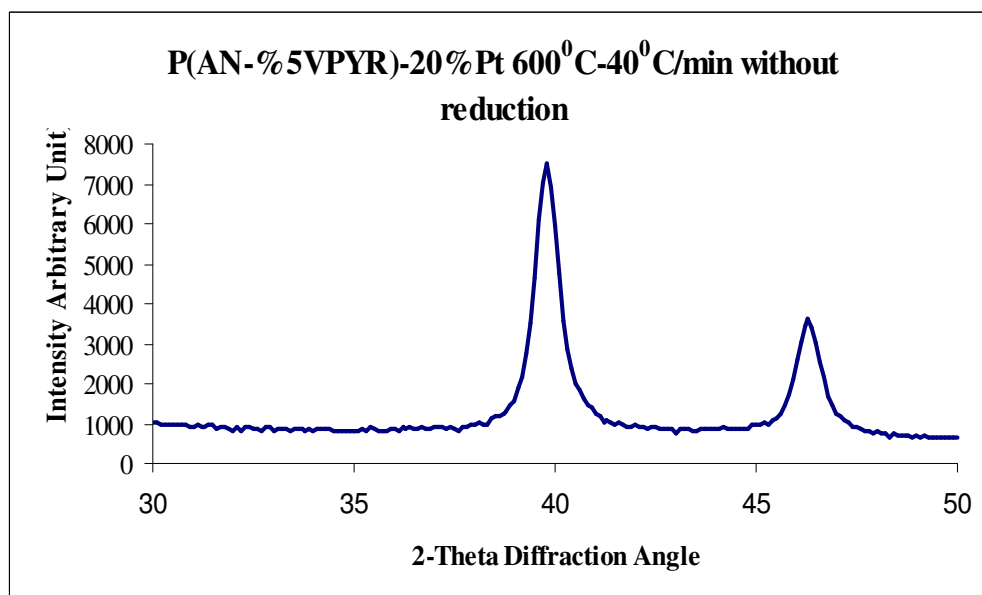
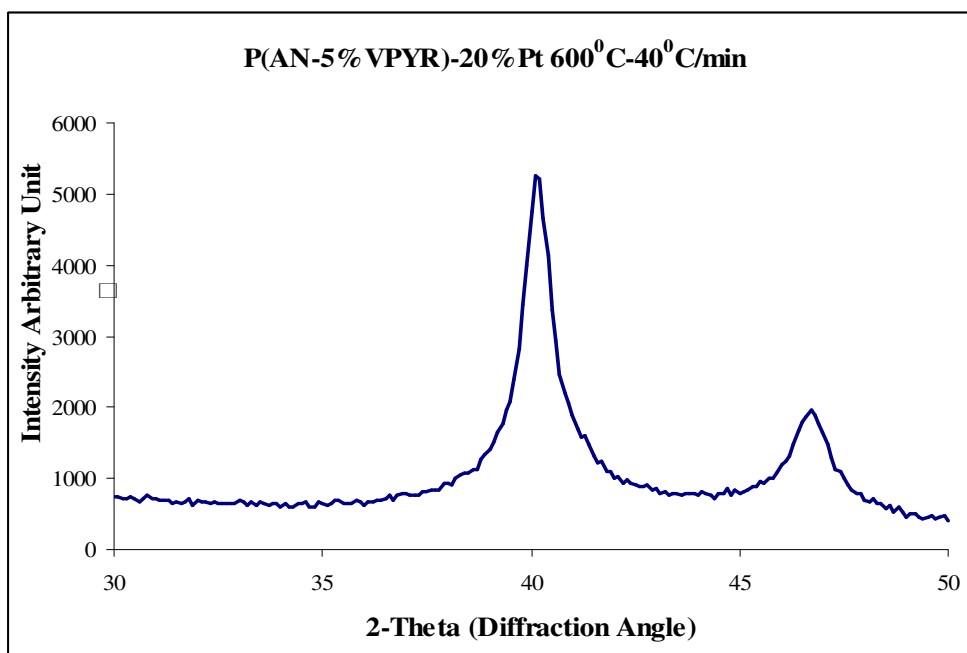


Figure 3.15-16. P(AN-5%VPYR)-20%Pt 600C-40C/min with reducing agent and without reducing agent.

In table 3.7, carbonization temperature was fixed at 600⁰C and Pt content and co-monomer ratio were changed and crystalline size of Pt was tabulated. As heating rates increase, the crystalline size decreases as well. Also, crystalline size decreases while the Pt content increases. It can be explain that, as heating rates are increased, the nano particles have not time to become agglomerate.

Polymer	Temperature (°C)	Heating Rate (°C/min)	fwhm(°)	Crystalline size(nm)
P(AN-co-5%-VPYR), 5%Pt	600	40	0,528	16
P(AN-co-10%- VPYR), 5%Pt	600	40	0,586	14,5
P(AN-co-5%-VPYR), 10%Pt	600	5	0,532	15,9
P(AN-co-10%- VPYR), 10%Pt	600	5	0,492	17,3
P(AN-co-5%-VPYR), 20%Pt	600	40	0,903	9,4
P(AN-co-10%- VPYR), 20%Pt	600	40	0,711	11,9

Table 3.7 Pt including copolymers with different comonomer and Pt ratios

It was observed that the crystalline size did not much depend on the comonomer ratio in copolymer. Therefore, P(AN-co-5%VPYR) was focused and studied in this research.

3.9.2. XRD Analysis of Pd including fibers

After carbonization process, Pd including fibers was analyzed via x-ray diffractometer to calculate crystalline sizes. Similar trends were observed in Pd nanoparticles: the crystalline sizes increased as the carbonization temperature increased.

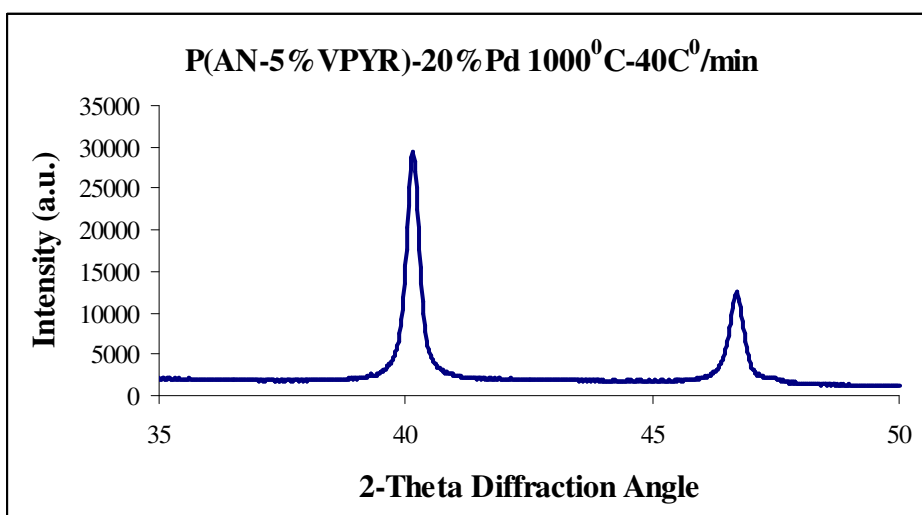


Figure 3.17. 20%Pd carbonized at 1000⁰C

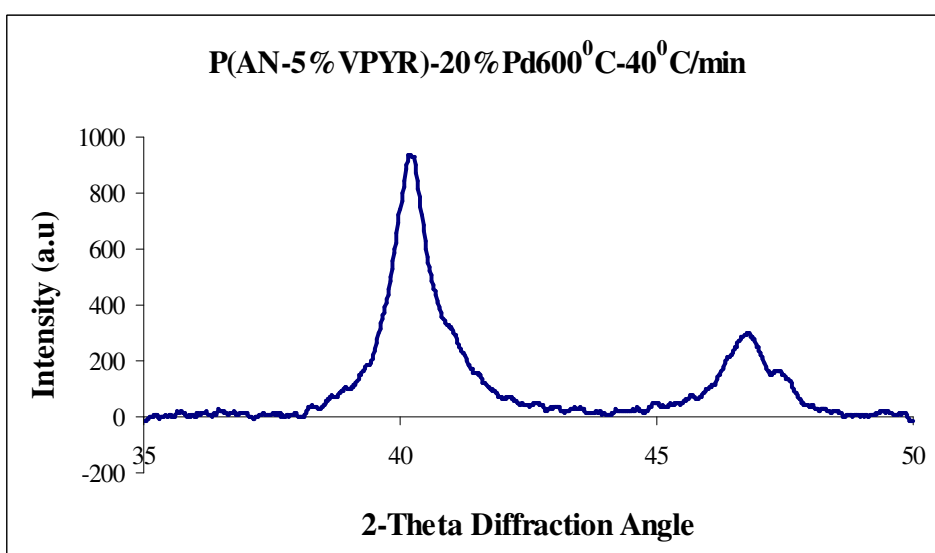


Figure 3.18. 20%Pd carbonized at 600⁰C

The crystalline size of sample 20%Pd carbonized at 600⁰C was calculated as 11 nm while, it was 22,8 nm for 20%Pd carbonized at 1000⁰C. In a very similar study, Kurpiewski et al., Pd including carbon nano fibers from PAN (Polyacrilonitrile) precursor was electrospun. In this research, the Pd crystalline sizes varied from 45 nm to 60 nm at 900⁰C [55].

SEM, TEM and XRD results showed that, fiber diameter, metal content, reducing agent and carbonization directly affect size and distrubiton of the nanoparticles.

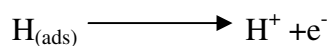
Moreover, it was proven that the co-monomer (VPYR) prevented the agglomeration of the metal particles in carbonization step. The electrostatic interaction between the side chain of the comonomer and the metal atom enabled the coordination [56]. Side chain ionic groups, bearing oxygen, nitrogen, sulfur, phosphorous and halogens are able to form a covalent bond with the metal by donating their lone pair 2p electrons to metal, which in turn metal back donates electrons from occupied d or f orbitals into empty Π^* -2p antibonding orbitals of ionic pendant groups.

3.10 Electrochemical Results

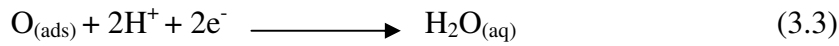
The electroactivity of the nanoparticles was determined both qualitatively and quantitatively by cyclic voltammetry. Cyclic voltammograms of all electrospun fibers that including nano Pt, Pd particles were recorded in 0,5M H₂SO₄ with various scan rate at room temperature and nitrogen atmosphere.

3.10.1 Electrochemical Analysis of Pt including fibers

The scanning was started from -0,25 V (SCE) and ending 1 V (SCE) which was common used range for fuel cell catalysts research [29]. Typical cyclic voltammogram of Pt catalysts was drawn in figure CV1. The first peak was at -0.2V (SCE), corresponded hydrogen desorption. Equation 3.1



At around 0.75V (SCE) oxide reduction region was reached after reverse sweeping was started (Equation 3.3). Here PtO is reduced and the second reaction is reversed (Equation 3.4).



Finally cathodic hydrogen - adsorption peaks occurred at -0.1V (SCE) (Equation 3.5).

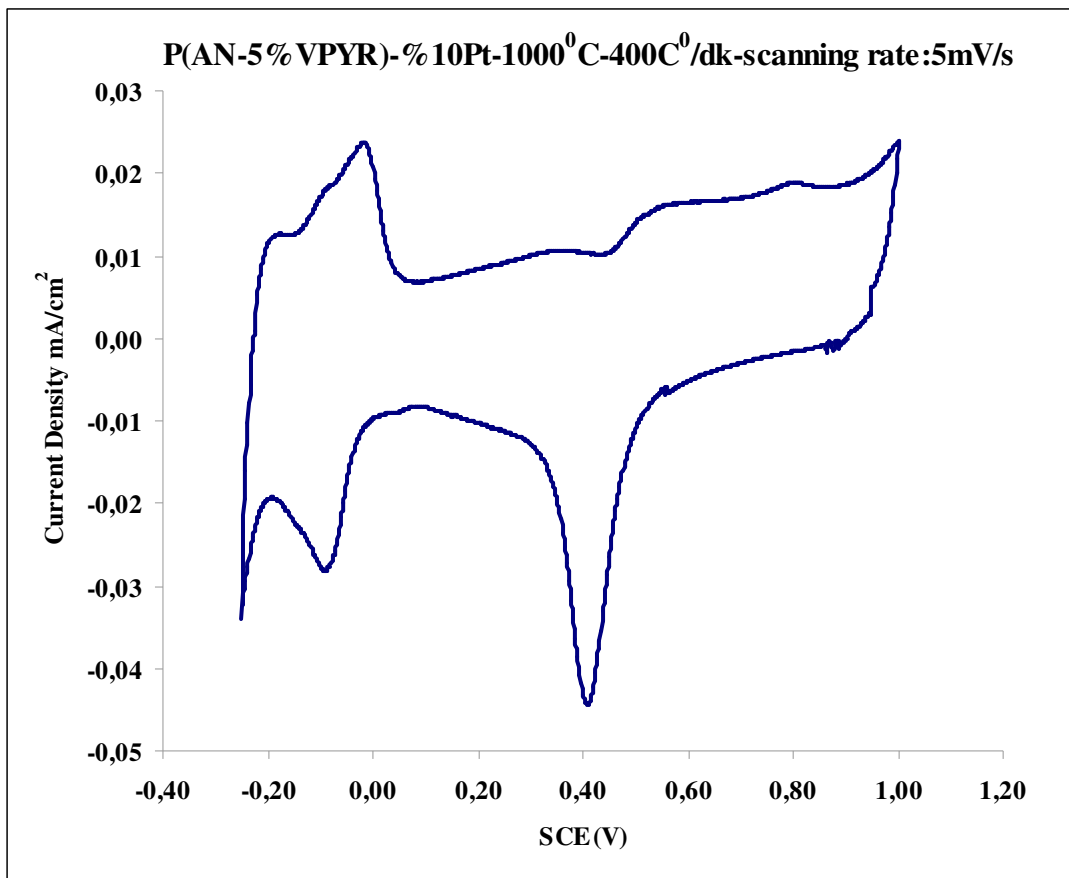


Figure 3.19. Cyclic Voltammogram of 20% Pt including carbon fiber

The shape of the cyclic voltammogram was the same as the polycrystalline platinum [57]. Hydrogen adsorption-desorption peaks were clearly seen in the voltammogram at the potentials between -0,2-0,05 V (SCE). Qualitatively, the voltmmogram showed the catalytical activity. For quantitative measurement, usually the charge under the hydrogen adsorption peak was used to calculate electrochemically

active surface area (formula 3) [58]. In some case, CO oxidation also is used in order to determine the active area [59].

$$\text{Electroactive Surface Area} = \text{ESA} = \frac{Q}{(Q_{\text{Pt Kristal}} \times m_{\text{Pt}})}$$

where,

Q: Hydrogen Adsorption Charge obtained from CV

Q_{Pt Kristal}: Charge for monolayer hydrogen adsorption on Pt ($210 \mu\text{C}/\text{cm}^2$) [60].

m_{Pt}: Pt amount that used in CV analysis

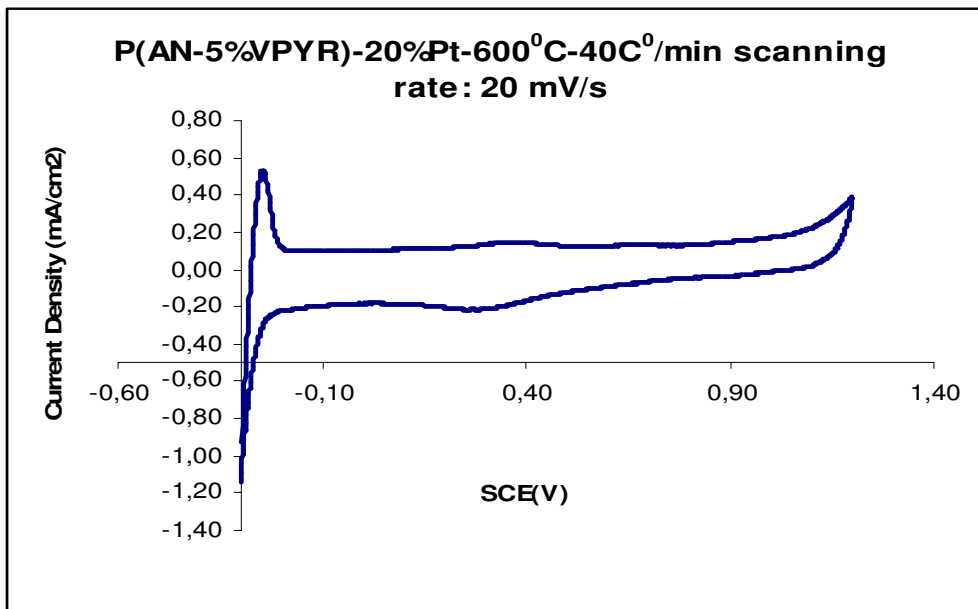


Figure3.20. P(AN-%5VPYR)-20%Pt 600°C 40C/min

The shape of the cyclic voltammogram in the figure3.9 was alike hydrogen oxidation peak was observed at -0,2V. Peak was associated with the weak bond of hydrogen in (111) Pt crystal direction.

Platinum Amount	Temperature°C	Electroactive Area	Average Particle Size (nm)
%5Pt	1200°C -5°C	21,4 m ² /g	10,1 nm
%10Pt	1000°C -40°C	31 m ² /g	5,2 nm
%20Pt	600°C -40°C	34,6 m ² /g	3,6 nm
%20Pt	1000°C -40°C	22 m ² /g	9,4 nm

Table 3.8. Summary of electrochemical results for Pt including fiber.

Highest electroactivity value 34,6 m²/g was achieved by 20% Pt including P(AN-5%VPYR) that was carbonized at 600⁰ C-40⁰C/min. The electroactive surface area of commercial Pt catalyst used in a PEMFC is around 70 m²/g [61]. Commercial Pt particle sizes do not exceed 4 nm [62]. Due to large agglomerated Pt nanoparticles, the electroactive area was achieved respectively lower. Furthermore, nanoparticles that were in the fibers were not electro-active. However, the electroactive surface area calculation is not only tool to qualify the catalysts. In order to evaluate the real performance of the nanocatalysts, real condition fuel cell testing is crucial.

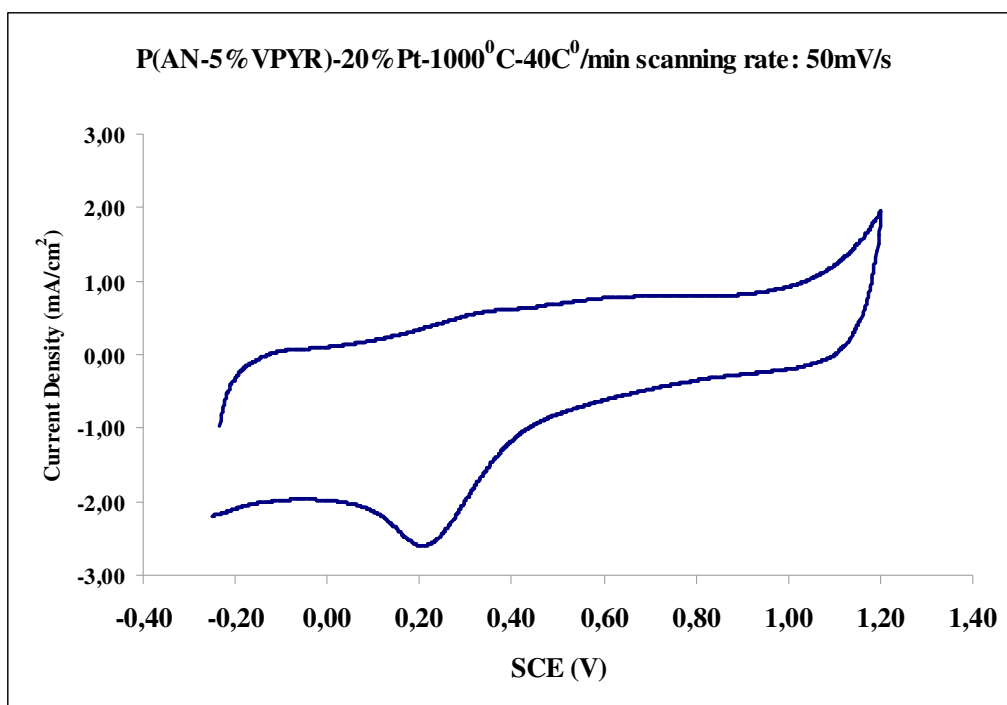


Figure 3.21 The behavior of Pt catalyst in oxygen saturated solution

In figure 3.10, the electrochemical behavior of Pt containing carbon fiber was observed in oxygen saturated sulphuric acid solution. Although, the oxygen reduction reaction should be examined under rotating voltammetry, the cyclic voltammogram gave an idea that the oxygen reduction reaction was completed [63].

3.10.2 Electrochemical Analysis of Pd including fibers

The peaks at Figure V are corresponded the electrochemical activity. For a positive sweep voltage starting from -0.25V (SCE) moving higher potential, the first peak after -0.2V(SCE) is the hydrogen desorption peak (Equation 3.1).



If the surface of the electrode was very smooth multiple peaks could be distinguished for desorption of monolayer. While sweeping higher voltage oxide formation of PdO is encountered at around 0.39 V(SCE) (Equation 3.2).

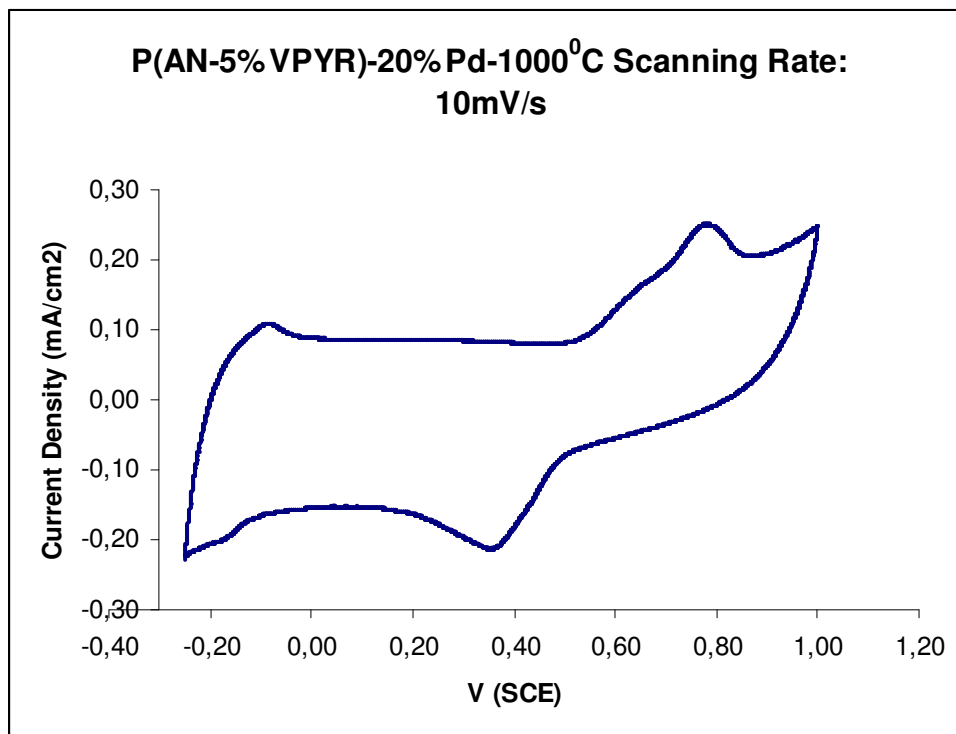
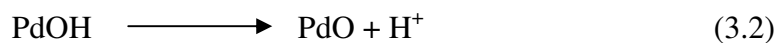
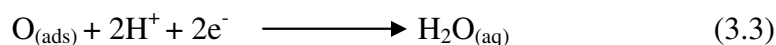


Figure 3.22. Cyclic voltammogram of slightly defined adsorption and desorption regions for hydrogen of Pd nanoparticles on carbon fibers at 10mV/s scan rate in 0.5M H_2SO_4 .

At around 0.75V (SCE) oxide reduction region was reached after reverse sweeping was started (Equation 3.3). Here PdO is reduced and the second reaction is reversed (Equation 3.4).



Finally cathodic hydrogen - adsorption peaks occurred at -0.1V (SCE) (Equation 3.5).



Different heating rates and heating temperature gave different voltammograms. If the Pd concentration increases the current density dramatically becomes greater. It is obvious that, as the Pd content per cm^2 area is higher changing from 5% to 20% with respect to polymer weight, more electro active sites will be available; as a result, more current can be obtained (Figure 3.23.) Also, the carbonization rate of the carbon fiber based Pd nanoparticles is directly related with the obtained current. Rapid carbonization yields agglomeration of Pd particles with lower currents for the samples heated to 600°C at a rate between $0.1^\circ\text{C}/\text{min}$ to $5^\circ\text{C}/\text{min}$. The Figure 3.23 confirms this fact.

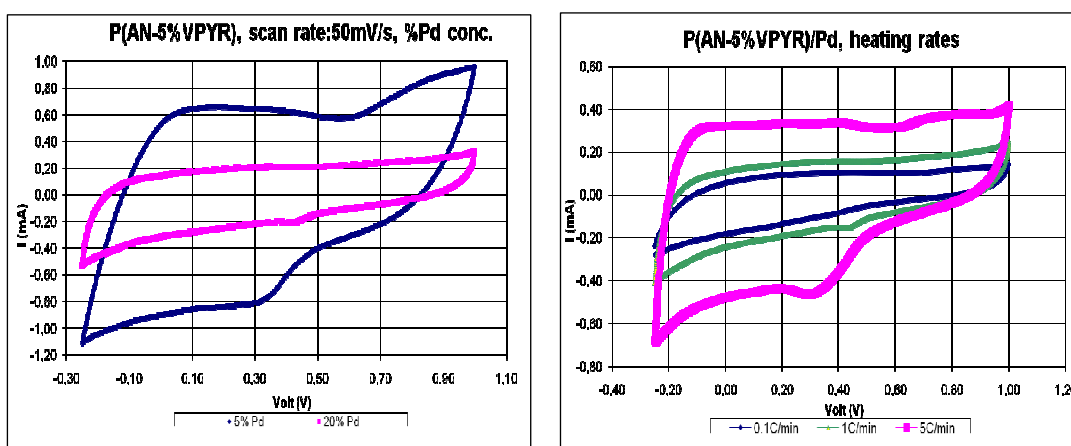


Figure 3.23. Cyclic voltammograms of P (AN-co-VPYR) carbon nanofibers a) at increasing Pd concentration (%5 Pd, %20 Pd in weight with respect to polymer b) at various heating rates ($0.1^\circ\text{C}/\text{min}$, $10^\circ\text{C}/\text{min}$, $50^\circ\text{C}/\text{min}$)

Electroactive surface area can be calculated via either hydrogen adsorption [58] or oxide reduction [64] peak at the cyclic voltammogram for Pd nanocatalysts. In this study, the oxide reduction peaks were investigated. Because, for Pd catalysts hydrogen molecules are not only adsorbed but also absorbed [64]. Electrochemical activity results for Pd catalysts were shown in table 3.30

Palladium Amount	Charge ($\mu\text{C}/\text{cm}^2$)	Electroactive Surface Area	Average Particle Size (nm)
%5Pd	287 $\mu\text{C}/\text{cm}^2$	22,37 m^2/g	<4; 28; $6\pm 4,9$
%10 Pd	507 $\mu\text{C}/\text{cm}^2$	12 m^2/g	$6,2\pm 0,9$; $14,9\pm 1,8$
%20 Pd	260 $\mu\text{C}/\text{cm}^2$	5,48 m^2/g	$6,3\pm 1,0$; $19,2\pm 3,2$

Table3.9. Summary of electrochemical results for Pd including fiber

Lower activity values were obtained from Pd including carbon nanofibers comparing Pt including carbon fibers. Indeed, Pt nanocatalysts are more active than Pd nanocatalysts. Pt catalysts or Pt-M binary catalysts are used currently in a PEMFC [65].

CHAPTER 4

CONCLUSION AND FUTURE WORKS

Fuel cells have become a favorable, future high efficient energy sources because they can convert chemical energy directly into electricity in an environmentally friendly manner. Among various types of fuel cells proton exchange membrane fuel cells (PEMFC), have emerged as candidates for transportation, portable and stationary systems due to their good energy efficiency and high power density. One of the significant challenge to commercial use of PEMFCs is the high cost of the noble catalysts. Increasing catalyst utilization may lead the decrease in the amount. An alternative catalyst supporter, carbon nanofibers not only enhances catalyst utilization but also reduce catalyst amount due to their high surface area and excellent electrical conductivity.

Platinum and Palladium metal nanocatalysts including carbon nanofibers for proton exchange membrane fuel cells were produced via electrospinning successfully. Polyacrylonitrile copolymers, P(AN-co-AA) and P(AN-co-VPYR) were synthesized by solution polymerization. Due to its alternating nature, P(AN-co-VPYR) polymer was focused and comprehensive study was conducted to understand the main parameters on the formation of carbon nanofibers and nanoparticles. The proposed study enabled to gain control on the particle size of metal particle on nanometric scale by manipulation of polymer chemistry, electrospinning parameters and carbonization procedures. By the optimization of variables, Pt and Pd metal size was reduced up to 5 nm while the fiber diameter was achieved as small as 20 nm. Furthermore, highest electrochemical activity was found as 34,6 m²/g for Pt catalyst, and 22,37 m²/g for Pd catalysts which shows that further improvements should be done in order to use these catalysts directly

in a proton exchange membrane fuel cell. Lower activities might stem from not only relatively bigger particles (20 nm), but also particles that were stayed in the fiber.

In order to activate, inner shell metal particles, porous fiber production will be tried. In a near future, the catalysts will be tested in a real fuel cell system, to investigate the real activity and behavior of the catalysts. In addition to this, rotating disc electrode studies will be employed to understand oxygen reduction kinetics. Binary Pt-Pd, Pt-Co including fibers will also be produced which followed by a comprehensive TEM analysis. Moreover, the behaviors of the catalysts and carbon fibers in a real fuel cell stack will be investigated.

REFERENCES

- [1] F. Barbir, "PEM Fuel Cells", Elsevier Academic Press, Burlington, MA, 2005.
- [2] W.R. Grove, "On voltaic series and the combination of gases by platinum", Phil. Mag. 14, 1839, pp. 127-130.
- [3] I. Parsons, "Fuel Cell Handbook", 5th edition, DOE, Morgantown, West Virginia, 2002.
- [4] J.O'M. Bockris, S. Srinivasan, "Fuel Cells –Their Electrochemistry", McGraw Hill, New York, 1969.
- [5] J. Larminie, A. Dicks, "Fuel Cell Systems Explained", 2nd edition, Wiley, New York, 2003.
- [6] B. C. H. Steele, A. Heinzl, "Materials for fuel cell technologies", Nature, Vol. 41, 2001, pp. 345-352.
- [7] K. Kordesh, S. Gunter, "Fuel cells and their applications", Berlin, Wiley, 1996.
- [8] G.F.Mclean, T. Niet, S.Prince-Richard, N.Djilali, "An assessment of alkaline fuel cell technology", International Journal of Hydrogen Energy, Vol. 27, pp. 507-526, 2002.
- [9] A. J. Appleby, "Fuel cell technology: Status and future prospects", Energy, Vol. 21, pp. 521-653, 1996.

- [10] S.R.Choudhury, M.B. Deshmukh, R. Rengaswamy, "A two-dimensional steady-state model for phosphoric acid fuel cells (PAFC) ' Journal of Power Sources, Vol. 112, pp. 137-152, 2002.
- [11] J.L.Silveira, E.M.Leal, L. Ragonha Jr., "Analysis of molten carbonate fuel cell: cogeneration to produce electricity and cold water", Energy, Vol. 26, pp. 891-904, 2001.
- [12] A.B.Stambouli, E.Traversa, "Solid oxide fuel cells (SOFCs): a review of an environmentally clean and efficient source of energy", Renewable and Sustainable Energy Reviews, Vol. 6, pp. 443-455, 2002.
- [13] W. Vielstich, A. Lamm, H.A. Gasteiger, "Handbook of Fuel Cells: Fundamentals Technology and Applications", Vol. 2, Wiley, New York, 2003.
- [14] V. Metha, J.S.Cooper, "Review and analysis of PEM fuel cell design and manufacturing", Journal of Power Sources, Vol. 114, pp. 32-53, 2003.
- [15] W. Vielstich, A. Lamm, H.A. Gasteiger, "Handbook of Fuel Cells: Fundamentals Technology and Applications", Vol. 3, Wiley, New York, 2003.
- [16] S. Litster, G. McLean, "PEM fuel cell electrodes" Journal of Power Sources, Vol. 130 (1-2), pp. 61-76, 2004.
- [17] P.Costamagna, S. Srinivasan, "Quantum jumps in the PEMFC science and technology from the 1960s to the year 2000 Part I. Fundamental scientific aspects", Journal of Power Sources, Vol. 102, pp. 242-252, 2001.
- [18] S. J. C. Cleghorn, X. Ren, T. E. Springer, M. S. Wilson, C. Zawodzinski, T. A. Zawodzinski and S. Gottesfeld, "PEM fuel cells for transportation and stationary power generation applications" International Journal of Hydrogen Energy, Vol. 22, pp. 1137-1144, 1997.
- [19] M.H. Sossina, "Fuel cell materials and components", Acta Materiala, Vol. 51, pp. 5981-6000, 2003.
- [20] D. Chu, R. Jiang, "Comparative studies of polymer electrolyte membrane fuel cell stack and single cell", Journal of Power Sources, Vol. 80, pp. 226-234, 1999.

[21] M. Rikukawa, K. Sanui, ‘‘Proton-conducting polymer electrolyte membranes based on hydrocarbon polymers’’, *Progress in Polymer Science*, Vol.25 (10), pp. 1463-1502, 2000.

[22] J. Zhang, Z. Xie, J. Zhang, Y. Tang, C. Song, T. Navessin, Z. Shi, D. Song, H. Wang, D. P. Wilkinson, Z. S. Liu and S. Holdcroft, ‘‘High temperature PEM fuel cells’’, *Journal of Power Sources*, Vol.160 (2), pp. 872-891, 2006.

[23] S. Litster and G. McLean, ‘‘PEM fuel cell electrodes’’, *Journal of Power Sources*, Vol.130 (1-2), pp. 61-76, 2004.

[24] V. Mehta and J.S. Cooper, ‘‘ Review and analysis of PEM fuel cell design and manufacturing’’, *Journal of Power Sources*, Vol.114, pp. 32–53, 2003.

[25] G.S. Kumar, M. Raja and S. Parthasarathy, ‘‘High performance electrodes with very low platinum loading for polymer electrolyte fuel cells’’, *Electrochimica Acta*, Vol. 40, pp. 285–290, 1995.

[26] M.S. Wilson, Membrane catalyst layer for fuel cells, U.S. Pat. No. 5,234,777 1993.

[27] Y.G. Chun, C.-S. Kim, D.-H. Peck and D.-R. Shin, ‘‘Performance of a polymer electrolyte membrane fuel cell with thin film catalyst electrodes’’, *Journal of Power Sources* Vol. 71, pp. 174–177, 1998.

[28] Y.G. Yoon, G.G. Park, T.-H. Yang, J.-N. Han, W.Y. Lee and C.-S. Kim, ‘‘ Effect of pore structure of catalyst layer in a PEMFC on its performance’’, *International Journal of Hydrogen Energy*, Vol. 28, pp. 657–662, 2003.

[29] M.S. Wilson and S. Gottesfeld, ‘‘Thin-film catalyst layers for polymer electrolyte fuel cell electrodes’’ *Journal of Applied Electrochemistry*, Vol.22, pp. 1–7, 1992.

- [30] V.A. Paganin, E.A. Ticianelli and E.R. Gonzalez, “ Development and electrochemical studies of gas diffusion electrodes for polymer electrolyte fuel cells” Journal of Applied Electrochemistry , Vol.26, pp. 297–304, 1996.
- [31] V. Mehta and J. S. Cooper, “Review and analysis of PEM fuel cell design and manufacturing” , Journal of Power Sources, Vol. 114 (1), pp. 32-5, 2003.
- [32] E.J. Taylor, E.B. Anderson and N.R.K. Vilambi, “Preparation of high-platinum-utilization gas diffusion electrodes for proton-exchange-membrane fuel cells” Journal of Electrochemical Society, Vol. 139, pp. 45-46, 1992
- [33] Z. Qi and A. Kaufman, “Improvement of water management by a microporous sublayer for PEM fuel cells”, Journal of Power Sources Vol. 109 (1-15), pp. 38-46, 2002.
- [34] R.H.Borgwardt, “Transportation Research Part D-Transport and Environment” Vol. 6, 199-207, 2001
- [35] C. Wang, M. Waje, X. Wang, J.M. Tang, R.C. Haddon and Y. Yan, “Proton exchange membrane fuel cells with carbon nanotube based electrodes”, Nano Letters, Nano Letters, Vol. 4, pp. 345-348, 2004.
- [36] A. Formhals, “Process and Apparatus for Preparing Artificial Threads”, US Patent 1975504, 1934.
- [37] J. Doshi, G. Srinivasan, D. Reneker, “A Novel Electrospinning Process”, Polymer News, Vol. 20, pp. 909-920, 1995.
- [38] J. Doshi, D. Reneker, “Electrospinning Process and Applications of Electrospun Fibers”, Journal of Electrostatics, Vol. 5, 151-160, 1995.
- [39] J.M.Deitzel, J. Kleinmeyer, D. Harris, Tan N. C. Beck, “The Effect of Processing Variables on the Morphology of Electrospun Nanofibers and Textiles”, Polymer, Vol. 42, 261-272, 2001.

- [40] H. L. Schreuder-Gibson, and P. Gibson, "Applications of Electrospun Nanofibers in Current and Future Materials", *ACS Symposium Series 918*, Chapter 9, 2006, pp. 122-123.
- [41] Z. Wangxi, L. Jie, W. Gang, "Evolution of structure and properties of PAN precursors during their conversion to carbon fibers", *Carbon*, Vol. 41, pp. 2805-2812, 2003.
- [42] B.D.Cullity, "Elements of X-Ray Diffraction", Addison-Wesley, MA, 1978.
- [43] M.A. Brett, A. Maria, "Electroanalysis", Oxford University Press, New York, 1998.
- [44] A. Wieckowski, E.R. Sav, "Catalysis and electrocatalysis at nanoparticle surfaces", Marcel Dekker, New York, 2003.
- [45] O.Nuyken and G.Lattermann, "Handbook of Polymer Synthesis Part: A", New York 1992.
- [46] M.Lewin and E.M. Pearce, "Hand Book of Fiber Science and Technology", Vol. IV, Marcel Dekker, New York, 1985.
- [47] P. L. Donald, L. M. Gary, and G. S. Kriz, Jr. "Infrared Spectroscopy". In *Introduction to spectroscopy: A guide for students of organic chemistry*. Phyladelphia: International Thomson Publishing, 1997.
- [48] A.S. Brar and R. Kumar, "Sequence determination of N-vinyl-2-pyrrolidone/acrylonitrile copolymers by NMR spectroscopy", *European Polymer Journal* Vol. 37, p. 1827, 2001.
- [49] R. Meghabar, A. Megherbi and M. Belbachir, "Maghnite-H⁺, an ecocatalyst for cationic polymerization of N-vinyl-2-pyrrolidone", *Polymer*, Vol. 44, p. 4097, 2003.
- [50] P. Bajaj, K.A. Gupta, "Acrylonitrile-Acrylic Acid Copolymers: Synthesis and Characterization", *Journal of Applied Polymer Science*, Vol. 49, p. 823, 1993.

[51] F. R. Mayo and F. M. Lewis, "A Basis for Comparing the Behavior of Monomers in Copolymerization; The Copolymerization of Styrene and Methyl Methacrylate", *Journal of American Chemical Society*, Vol. 66 (9), pp. 1594-1601, 1944.

[52] H. Fong, I. Chun, D. H. Reneker, "Beaded Nanofibers Formed during Electrospinning", *Polymer*, Vol. 40, pp. 4585-4592, 1999.

[53] Y. Xiong, H. Cai, B. J. Wiley, J. Wang, M. J. Kim, and Y. Xia "Synthesis and Mechanistic Study of Palladium Nanobars and Nanorods" *American Chemical Society*, Vol. 129 (12), pp. 3665 – 3675, 2007.

[54] Z. Liu, L. M. Gan, L. Hong, W. Chen, J. Y. Lee, "Carbon-supported Pt nanoparticles as catalysts for proton exchange membrane fuel cells", *Journal of Power Sources*, Vol. 139, pp. 73-78, 2005.

[55] J. P. Kurpiewski,, "Electrospun Carbon Nanofiber Electrodes Decorated with Palladium Metal Nanoparticles: Fabrication and Characterization", (M.S), MIT, 2005.

[56] H. K. Lee, E. H. Jeong, C. K. Baek and J. H. Youk, "One-step preparation of ultrafine poly(acrylonitrile) fibers containing silver nanoparticles" *Materials Letters*, Vol. 59 (23), pp. 2977-2980, 2005.

[57] C. H. Hamann, A. Hamnett, W. Vielstich, "Electrochemistry", Wiley, New York, 1998.

[58] M. Chen, Y. Xing, "Polymer-Mediated Synthesis of Highly Dispersed Pt Nanoparticles on Carbon Black", *Langmuir*, Vol. 21, pp. 9334-9338, 2005.

[59] T. Vidakovic, C. Mihai, S. Kai, "The use of CO stripping for in situ fuel cell catalyst characterization", *Electrochimica Acta*, Vol. 52, pp. 5606-5613, 2007.

[60] R. Woods, "Hydrogen adsorption on platinum, iridium and rhodium electrodes at reduced temperatures and the determination of real surface area" *Journal of Electroanalytical Chemistry*, Vol. 49 (2), pp. 217-226, 1974.

[61] S. Gamburgzev and A.J. Appleby, "Recent progress in performance improvement of the proton exchange membrane fuel cell (PEMFC)", *Journal of Power Sources*, Vol. 107, pp. 5–12, 2002.

[62] Z. Qi and A. Kaufman, "Low Pt loading high performance cathodes for PEM fuel cells", *Journal of Power Sources*, Vol. 113, pp. 37–43, 2003.

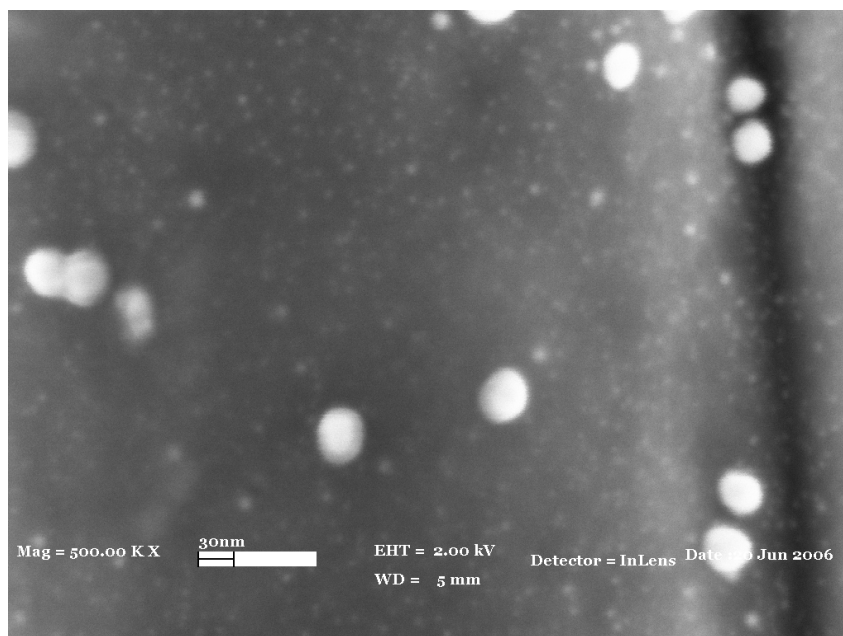
[63] M. Peuckert, "Oxygen Reduction on Small Supported Platinum Particles", *Journal of Electrochemical Society*, Vol. 133 (5), pp. 944-947, 1986.

[64] R., Pattabiraman, "Electrochemical investigations on carbon supported palladium catalysts *Applied Catalysis A:General*", Vol. 153, pp. 9-20, 1997.

[65] J. Moreira, P. Angel, A. L. Ocampo, P. J. Sebastian, J. A. Montoya, R. H. Castellanos, "Synthesis, characterization and application of a Pd/Vulcan and Pd/C catalyst in PEM fuel cell", *International Journal of Hydrogen Energy*, Vol. 29, pp. 915-920, 2004.

APPENDIX

(a)



(b)

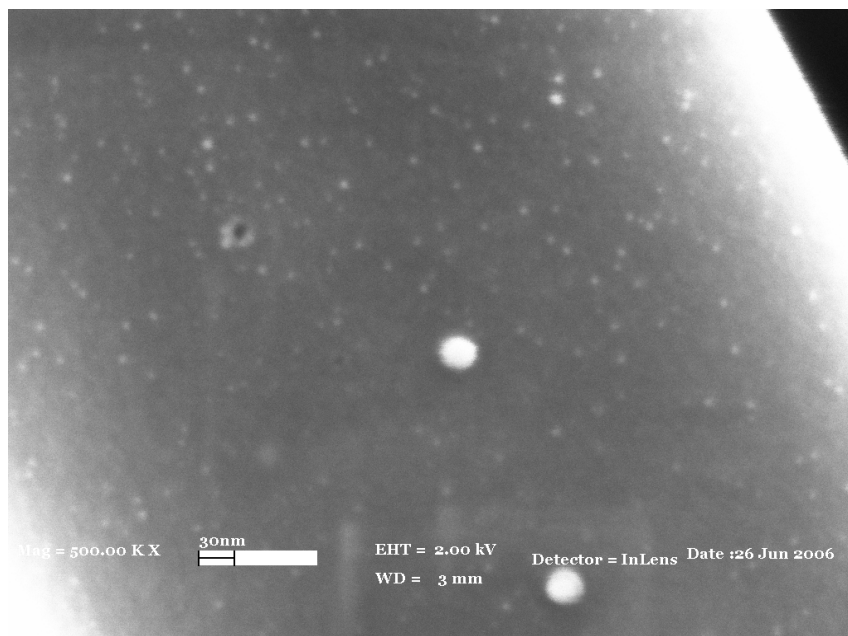
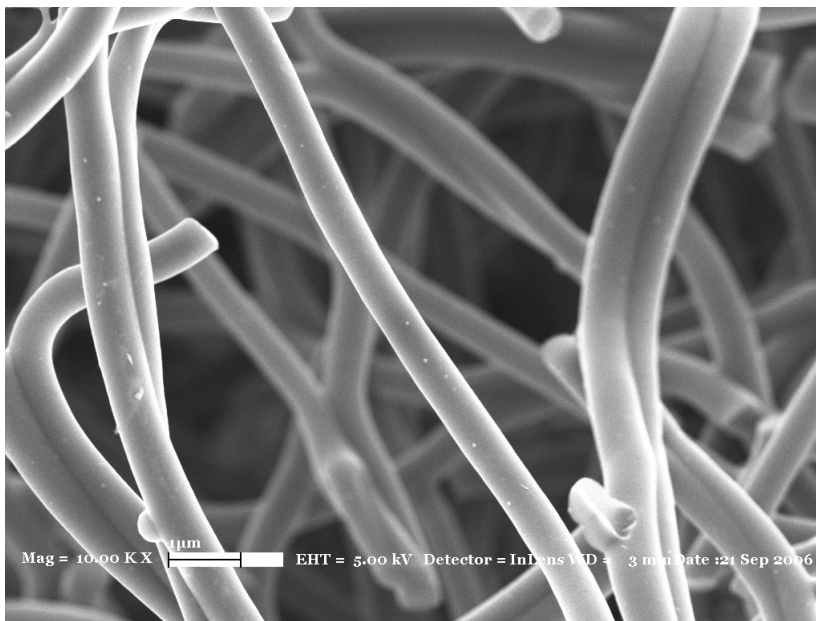


Figure A.1. (a) 0.1 °C/min heating rate, (b) 1 °C/min heating rate for P(AN-co-%5-VPYR), 5%Pd 600°C

(a)



(b)

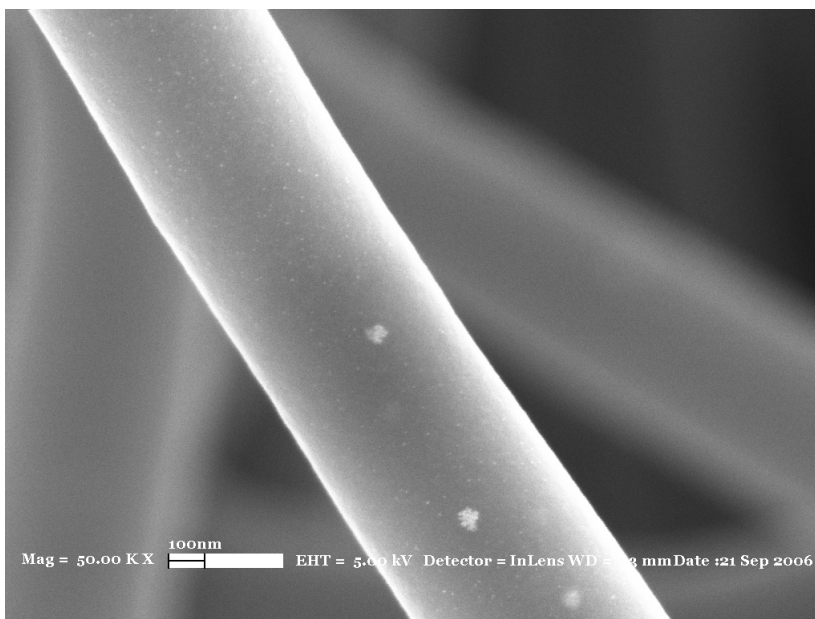
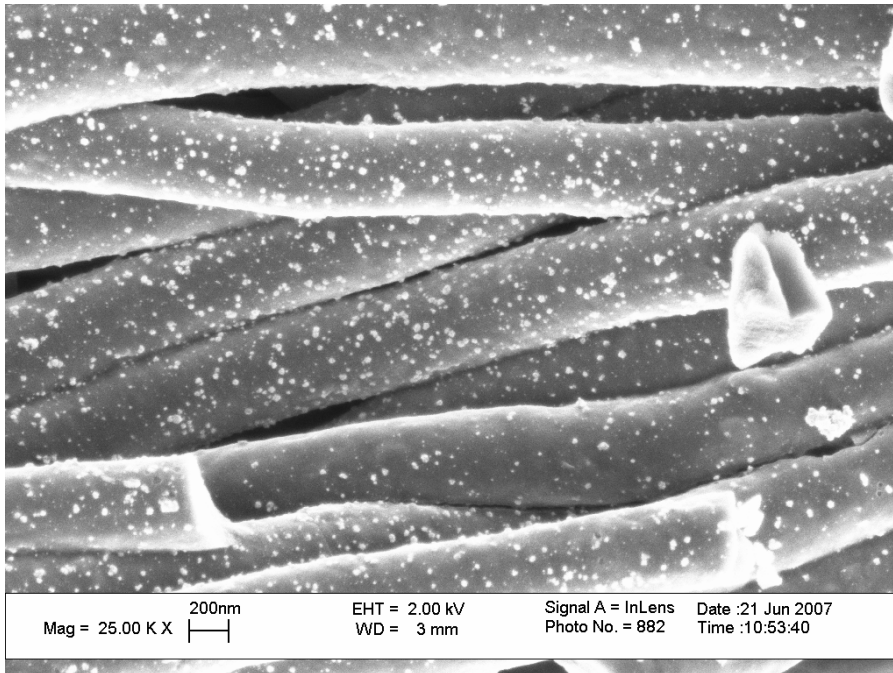


Figure A.2. P(AN-co-5-VPYR), 20%Pd 600⁰C- 40⁰C/min, 2 distributions

(a)



(b)

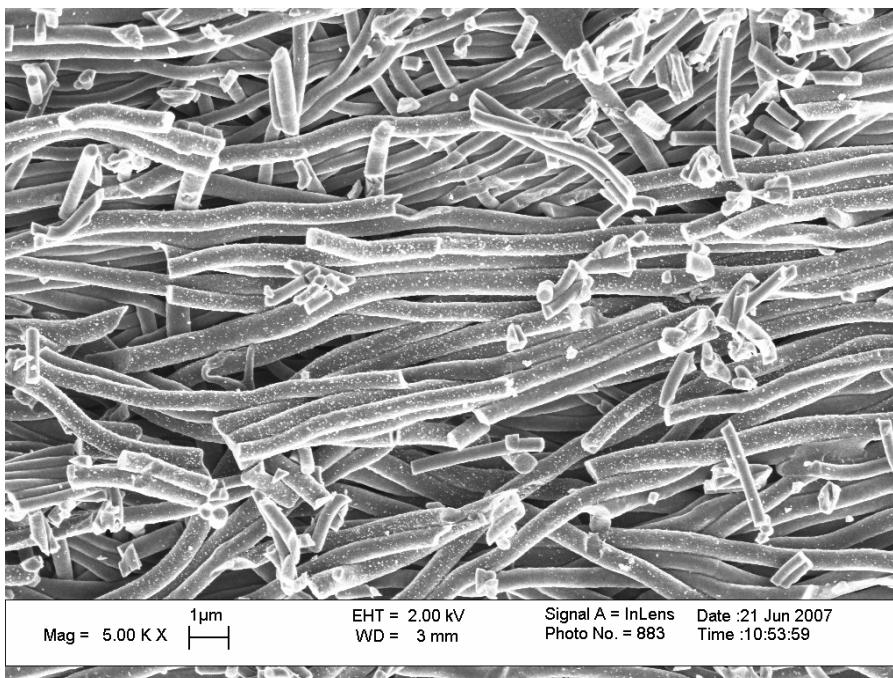


Figure A.3. P(AN-co-5-VPYR), 20%Pt 600⁰C- 40⁰C/min, different magnification.

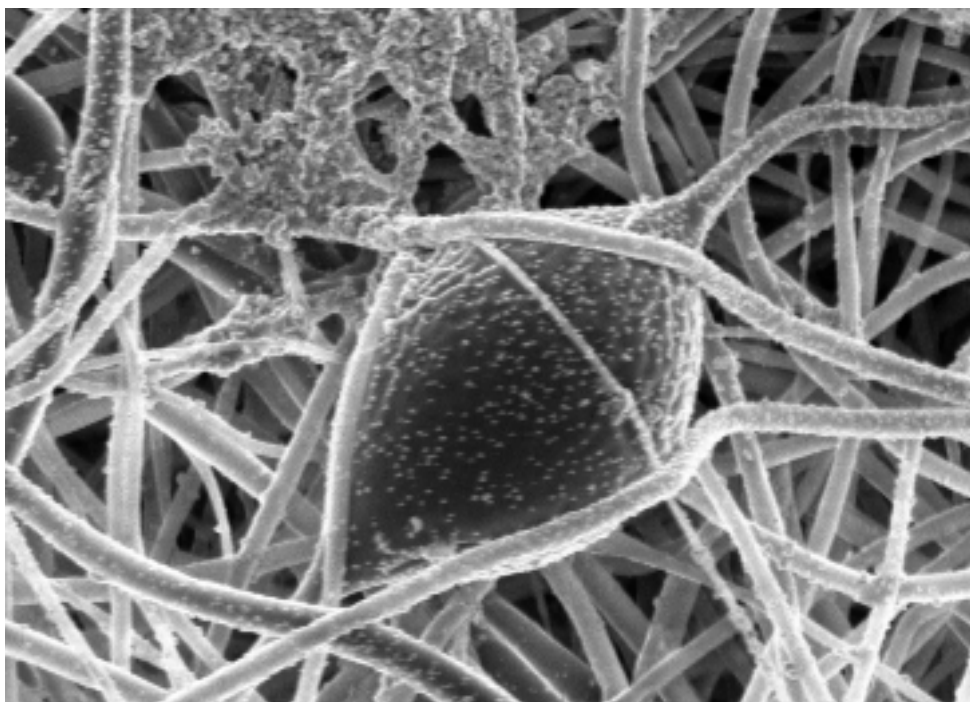


Figure A.4. P(AN-co-%5-VPYR), 20%Pt 600⁰C- 40⁰C/min, bead formation, 8% polymer concentration (lower polymer concentration)

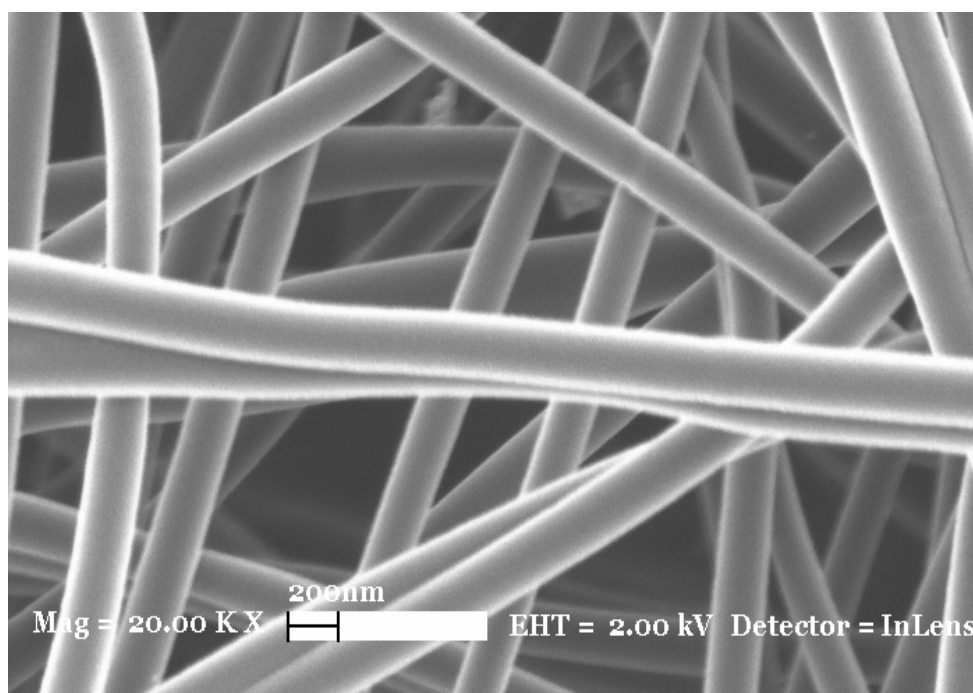


Figure A.5. P(AN-co-%5-VPYR), 20%Pt 600⁰C- 40⁰C/min, unreduced, smooth fiber formation , 15% polymer concentration (higher polymer concentration)

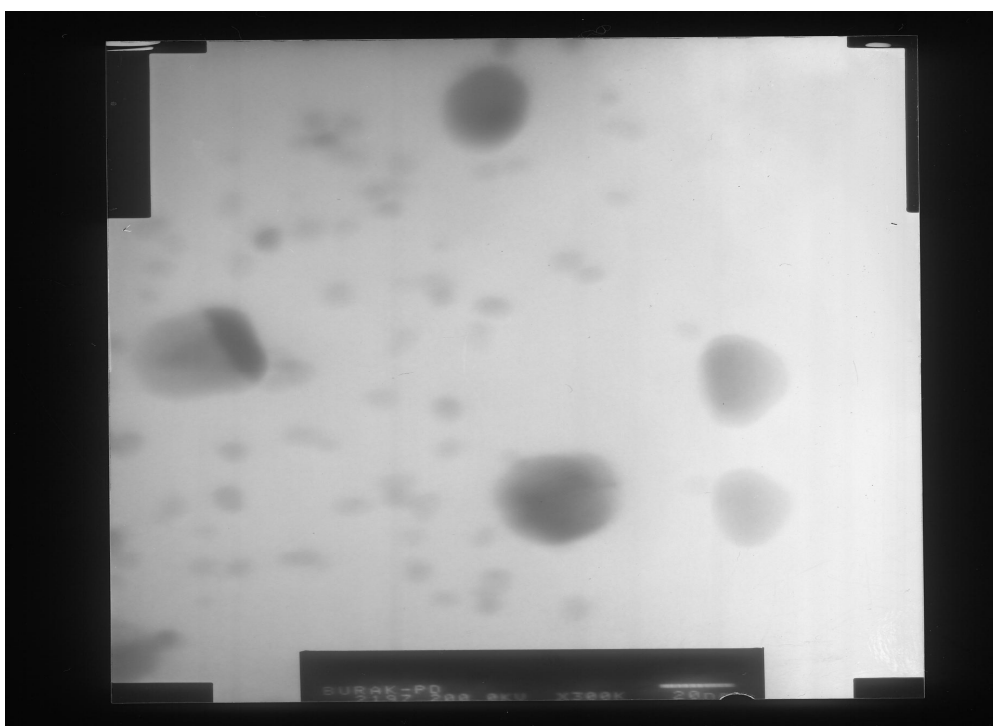
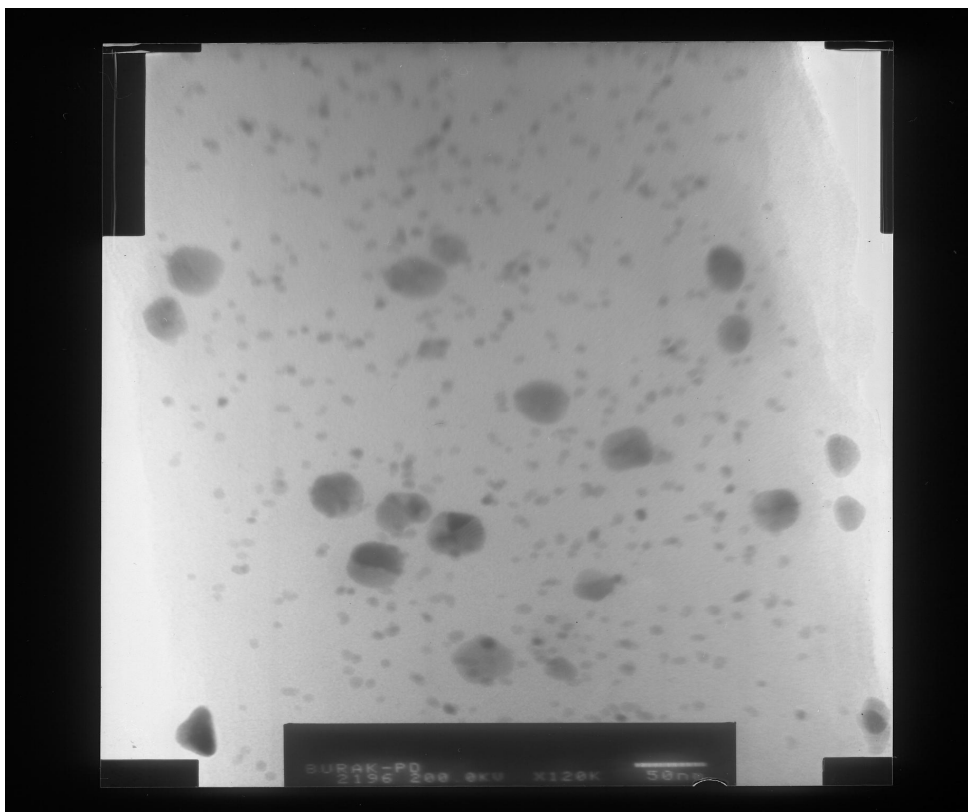


Figure A.6. TEM of P(AN-co-%5-VPYR), 20%Pd 1000⁰C- 40⁰C/min, 2 Distrubitions 3-5 nm, 20-40 nm